




ARTICLE

# N-cadherin signaling via Trio assembles adherens junctions to restrict endothelial permeability

Kevin Kruse<sup>1</sup>, Quinn S. Lee<sup>1</sup>, Ying Sun<sup>1</sup>, Jeff Klomp<sup>1</sup>, Xiaoyan Yang<sup>1</sup>, Fei Huang<sup>1</sup>, Mitchell Y. Sun<sup>1</sup>, Shuangping Zhao<sup>1</sup>, Zhigang Hong<sup>1</sup>, Stephen M. Vogel<sup>1</sup>, Jae-Won Shin<sup>1</sup>, Deborah E. Leckband<sup>3</sup> , Leon M. Tai<sup>2</sup>, Asrar B. Malik<sup>1</sup> , and Yulia A. Komarova<sup>1</sup> 

**Vascular endothelial (VE)-cadherin forms homotypic adherens junctions (AJs) in the endothelium, whereas N-cadherin forms heterotypic adhesion between endothelial cells and surrounding vascular smooth muscle cells and pericytes. Here we addressed the question whether both cadherin adhesion complexes communicate through intracellular signaling and contribute to the integrity of the endothelial barrier. We demonstrated that deletion of N-cadherin (*Cdh2*) in either endothelial cells or pericytes increases junctional endothelial permeability in lung and brain secondary to reduced accumulation of VE-cadherin at AJs. N-cadherin functions by increasing the rate of VE-cadherin recruitment to AJs and induces the assembly of VE-cadherin junctions. We identified the dual Rac1/RhoA Rho guanine nucleotide exchange factor (GEF) Trio as a critical component of the N-cadherin adhesion complex, which activates both Rac1 and RhoA signaling pathways at AJs. Trio GEF1-mediated Rac1 activation induces the recruitment of VE-cadherin to AJs, whereas Trio GEF2-mediated RhoA activation increases intracellular tension and reinforces Rac1 activation to promote assembly of VE-cadherin junctions and thereby establish the characteristic restrictive endothelial barrier.**

## Introduction

The endothelium lining vessels forms a physical barrier between the circulating blood and interstitium that restricts in a size-selective manner the passage of solutes and plasma proteins (Komarova et al., 2017). This specific property of the endothelium is attributed to vascular endothelial (VE)-cadherin junctions (known as adherens junctions [AJs]) located between endothelial cells (ECs; Simionescu et al., 1975; Del Vecchio et al., 1987; Mehta and Malik, 2006). In addition to VE-cadherin, ECs also express N-cadherin (Lampugnani et al., 1992; Salomon et al., 1992), which forms heterotypic adhesions with surrounding pericytes or vascular smooth muscle cells (Salomon et al., 1992; Navarro et al., 1998; Frye et al., 2015). Endothelial-specific deletion of either *Cdh2* (N-cadherin) or *Cdh5* (VE-cadherin) increases vascular permeability in mice and causes lethality in embryos at embryonic day 9.5 due to defective vascularization (Carmeliet et al., 1999; Luo and Radice, 2005). Thus, both cadherins contribute to establishing the VE barrier, although N-cadherin has a unique role in recruiting pericytes during neonatal and postnatal angiogenesis (Gerhardt et al., 2000; Tillet et al., 2005). Pericytes localized at entry points of AJs are thought to stabilize the microvessel junctional barrier (Alimperti et al., 2017). Studies also show that N-cadherin up-regulates VE-cadherin protein expression (Luo

and Radice, 2005) through a yet unknown mechanism. These raise intriguing questions as to the mechanisms of N-cadherin-mediated assembly of VE-cadherin and the role of N-cadherin-activated signaling in endothelial barrier function.

Here we investigated the role of N-cadherin in the formation of VE-cadherin junctions following the inducible deletion of N-cadherin in ECs or pericytes in mice. We identified a crucial N-cadherin-activated signaling pathway responsible for the assembly of AJs. N-cadherin functioned by interacting with and activating Trio, a dual Rac1/RhoA guanine nucleotide exchange factor (GEF). Rac1 activation induced recruitment of VE-cadherin to AJs, whereas RhoA increased myosin II activity to reinforce the activation of Rac1 at AJs. Thus, coordinated activation of both Rac1 and RhoA by N-cadherin-associated Trio is essential for the formation of a restrictive endothelial barrier.

## Results

### Deletion of N-cadherin in ECs and pericytes increases junctional permeability in mice

Studies were made in mice in which *Cdh2* gene was deleted in ECs using the inducible tamoxifen-responsive Cre/loxP

<sup>1</sup>Department of Pharmacology, University of Illinois College of Medicine, Chicago, IL; <sup>2</sup>Department of Anatomy and Cell Biology, University of Illinois College of Medicine, Chicago, IL; <sup>3</sup>Department of Chemical and Biomolecular Engineering, University of Illinois at Urbana-Champaign, Urbana, IL.

Correspondence to Yulia A. Komarova: [ykomarov@uic.edu](mailto:ykomarov@uic.edu).

© 2018 Kruse et al. This article is distributed under the terms of an Attribution-Noncommercial-Share Alike-No Mirror Sites license for the first six months after the publication date (see <http://www.rupress.org/terms/>). After six months it is available under a Creative Commons License (Attribution-Noncommercial-Share Alike 4.0 International license, as described at <https://creativecommons.org/licenses/by-nc-sa/4.0/>).

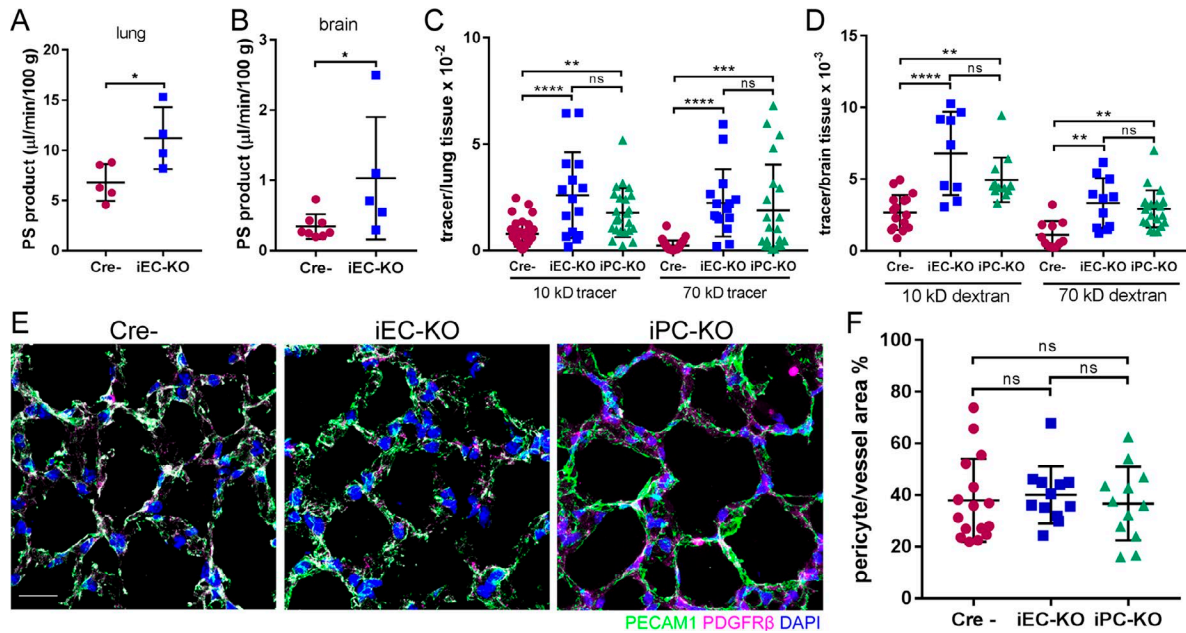


**Figure 1. *Cdh2* deletion in ECs and pericytes increases junctional endothelial permeability.** (A and B) Permeability times surface area (PS), a measure of transendothelial <sup>125</sup>I-albumin permeability, in lung (A) and brain (B) of Cre-negative (Cre<sup>-</sup>) control and *Cdh2* iEC-KO littermates. The data are expressed as the rate of <sup>125</sup>I-albumin leakage normalized to the dry weight of the tissue; *n* = 4–8 mice per group. \*, *P* < 0.05, a two-tailed, unpaired *t* test. (C and D) Measurement of lung (C) and brain (D) transendothelial permeability using 10-kD and 70-kD fluorescent dextran tracers. Data are presented as ratio of volume of fluorescent tracer to volume of lung or brain tissue for Cre<sup>-</sup>, *Cdh2* iEC-KO, and *Cdh2* iPC-KO mice. *n* = 10–15 fields from three to four mice per group. \*\*, *P* < 0.01; \*\*\*, *P* < 0.001; \*\*\*\*, *P* < 0.0001, ANOVA with Tukey's post hoc test. (E) 3D projected images of lung tissue from Cre<sup>-</sup>, *Cdh2* iEC-KO, and *Cdh2* iPC-KO mice stained for endothelial (PECAM1; green), pericyte (PDGFRβ; magenta), and nuclear (DAPI; blue) markers. Bar, 10 µm. (F) Quantification of pericyte coverage of lung microvessels expressed as pericyte area per vessel area (PDGFRβ/PECAM1) using images in E; *n* = 12–16 fields from three to four mice per group. ns, ANOVA with Tukey's post hoc test. (A–D and F) Data are shown as mean ± SD. See also Fig. S1.

recombination system (Gu et al., 1994). Here we crossed *Cdh2*<sup>fllox/fllox</sup> mice (Luo and Radice, 2005) with endothelial specific *end-SCL-Cre-ERT2* mice (Göthert et al., 2004) to generate *Cdh2*<sup>fllox/fllox/end-SCL-Cre-ERT2</sup> mice (iEC-KO). *Cdh2* was deleted in 6–8-wk-old mice, and the effects of *Cdh2* deletion were investigated as early as 2 wk after *Cre* induction (Fig. S1, A and B). These mice demonstrated no gross phenotype or reduction in lifespan. In contrast to embryonic lethality seen with conditional N-cadherin deletion in ECs due to down-regulation of VE-cadherin expression (Luo and Radice, 2005), inducible deletion of N-cadherin in ECs of adult mice had no effect on expression of either VE-cadherin or p120-catenin (Fig. S1, C and D). We observed that N-cadherin was absent on the abluminal surface of ECs in *Cdh2* iEC-KO mice, whereas it was expressed normally in control ECs (Fig. S1 E).

EC-specific deletion of N-cadherin increased basal permeability of both lung vessels to albumin from 6.8 ± 0.8 to 11.2 ± 1.5 µl/min/100 g (*P* = 0.0308) and brain vessels from 0.3 ± 0.1 to 1.0 ± 0.4 µl/min/100 g (*P* = 0.0488), respectively (Fig. 1, A and B). To address whether increased vascular permeability depended on the size of the tracer, in lieu of the albumin tracer used in the above experiments, we also used low (10-kD) and high (70-kD) molecular weight dextran tracers. In *Cdh2* iEC-KO mice, we observed increased basal vascular permeability to both dextran tracers as compared with basal vascular permeability values in control mice (Fig. 1, C and D; and Fig. S2 A). The lower permeability values of brain vessels compared with lung vessels are consistent with the greater restrictiveness of

the blood–brain barrier as compared with other vascular beds (Armulik et al., 2010).

Next, to determine whether the increased endothelial permeability phenotype in *Cdh2* iEC-KO mice can be reproduced following inducible deletion of *Cdh2* in pericytes, we also generated *Cdh2*<sup>fllox/fllox</sup>/PDGFRβ-P2A-CreER<sup>T2</sup> mice (Cuervo et al., 2017), termed iPC-KO (Fig. S1, F–I). iPC-KO mice also showed increased vascular permeability to dextran tracers as compared with control mice (Fig. 1, C and D; and Fig. S2 A). Thus, heterotypic N-cadherin trans-interaction between ECs and pericytes is required for restricting junctional permeability. Both KO mice also demonstrated increased permeability of pulmonary capillaries to fibrinogen (340 kD), an even larger protein than albumin, as evident from immunofluorescent staining (Fig. S2 B).

Since heterotypic N-cadherin adhesion may be required for contact between ECs and pericytes (Gerhardt et al., 2000; Daneman et al., 2010; Li et al., 2011; Frye et al., 2015), which, if reduced, could also explain the increased permeability (Armulik et al., 2010) seen in the N-cadherin KO mice described above, we next determined whether N-cadherin deficiency itself resulted in loss of pericyte coverage in capillaries. We observed that deleting N-cadherin in either ECs or pericytes did not reduce the number of pericytes covering ECs (Fig. 1, E and F; and Fig. S2, C and D).

### N-cadherin signaling promotes assembly of VE-cadherin junctions and restricts junctional permeability

To address whether the increased junctional permeability in *Cdh2* iEC-KO and iPC-KO mice shown above is coupled to alterations in

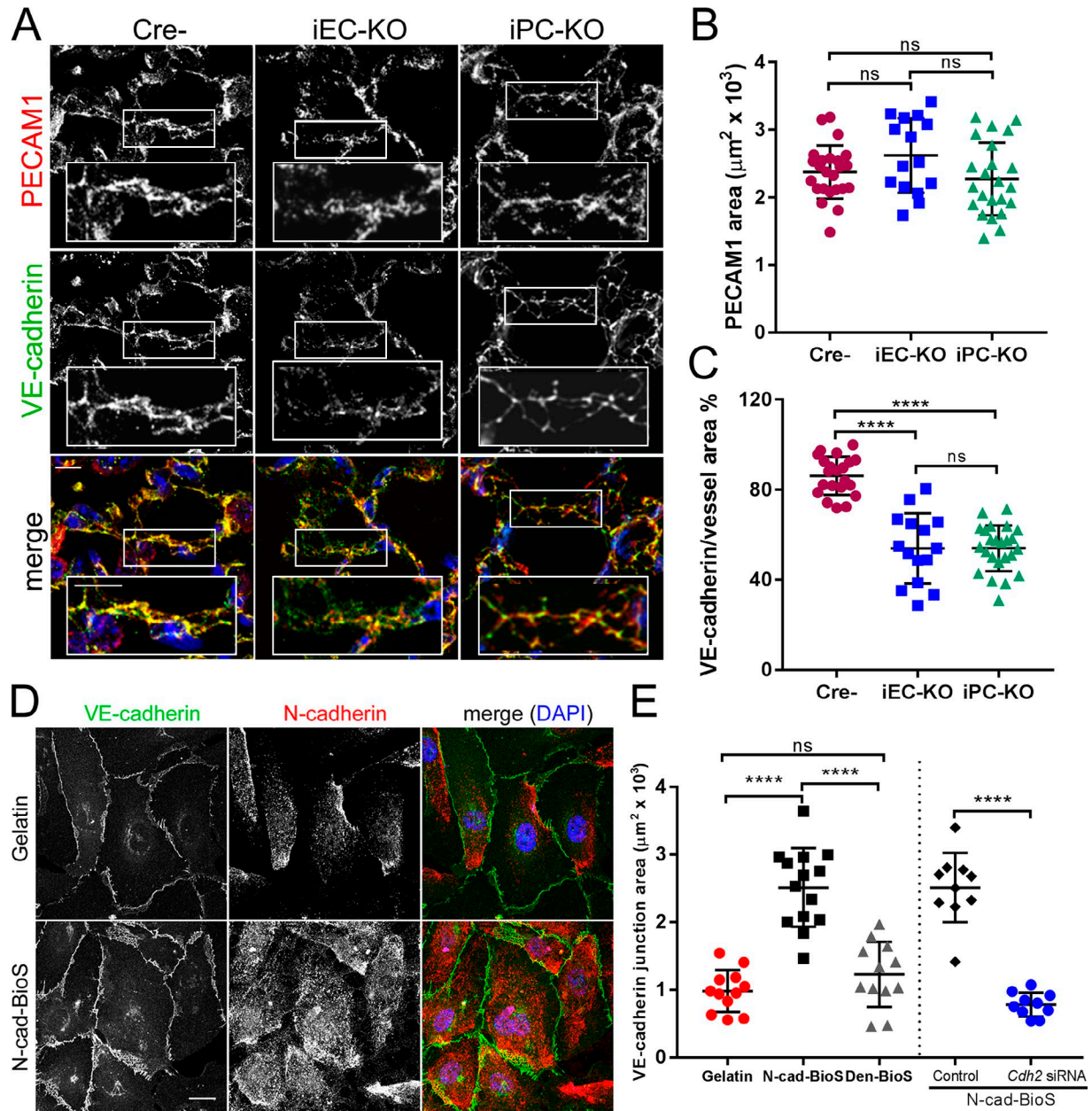


**Figure 2. N-cadherin adhesion signals assembly of VE-cadherin junctions.** (A) Representative confocal images of mouse lung sections from Cre<sup>-</sup>, *Cdh2* iEC-KO, and *Cdh2* iPC-KO mice stained for VE-cadherin (green on merged image), PECAM1 (red), and nuclei (DAPI, blue). Bar, 10  $\mu$ m; insets, 5  $\mu$ m. VE-cadherin at PECAM1-positive junctions is reduced in *Cdh2* iEC-KO and *Cdh2* iPC-KO mice as compared with controls. (B and C) Quantification of PECAM1 area (B) and VE-cadherin adhesion area normalized to PECAM1 area (C) in lungs of Cre<sup>-</sup>, *Cdh2* iEC-KO, and *Cdh2* iPC-KO mice;  $n = 15$ –26 images from three mice per group. \*\*\*\*,  $P < 0.0001$ , ANOVA with Tukey's post hoc test. (D) Representative confocal images of human pulmonary arterial ECs (HPAECs) grown on either gelatin-coated glass or N-cad-BioS and stained for VE-cadherin (green), N-cadherin (red), and DAPI (blue). Bar, 10  $\mu$ m. An anti-N-cadherin antibody targeting the cytosolic domain of N-cadherin was used to avoid staining of N-cad-BioS surface. (E) Quantification of VE-cadherin adhesion area from images in D; additional groups included denatured (Den) N-cad-BioS or N-cadherin depletion.  $n = 10$ –14 images per group. \*\*\*\*,  $P < 0.0001$ , ANOVA with Tukey's post hoc test. (B, C, and E) Data are shown as mean  $\pm$  SD. See also Fig. S2.

VE-cadherin at AJs, we performed confocal microscopic analysis of VE-cadherin junctions. We observed 40% reduction in VE-cadherin density at AJs in lung and brain endothelia of both KO models (Fig. 2, A–C; and Fig. S3, A and B). However, VE-cadherin and p120-catenin protein expression in ECs of pulmonary vessels was unchanged (Fig. S1, A–D).

To identify the N-cadherin adhesion signaling responsible for assembling VE-cadherin junctions, we developed an N-cadherin

biomimetic platform (N-cad-BioS) by covalently attaching the extracellular domain of N-cadherin in an oriented manner to a glass substrate (Fig. S3, C and D). This system enabled the formation of a confluent endothelial monolayer that interacted with the immobilized N-cadherin (Fig. S3, C and D). Using total internal reflection fluorescence (TIRF) microscopy to visualize ECs on N-cad-BioS, we observed clustering of N-cadherin on the abluminal surface and an increased concentration of N-cadherin clusters at the abluminal

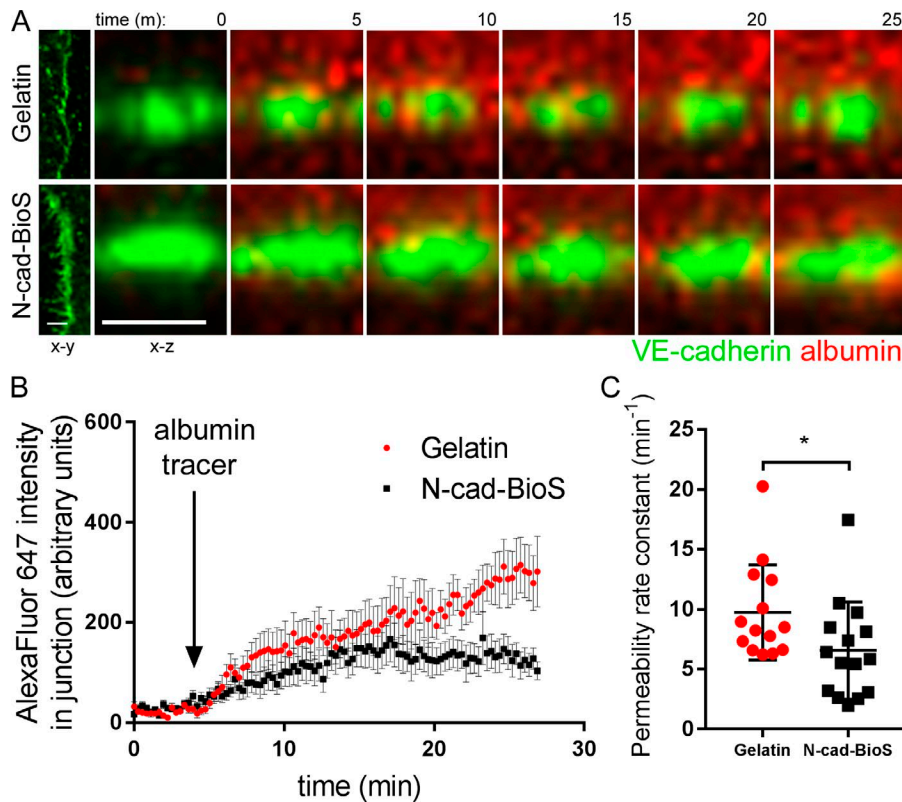


**Figure 3. N-cadherin-activated signaling restricts junctional permeability to albumin.** (A) Confocal live cell imaging of HPAECs expressing VE-cadherin-GFP (green) showing albumin-Alexa Fluor 647 (red) permeation across AJs. x-y (left) and x-z (enlarged, shown over time) sectional area of VE-cadherin-GFP junction. Albumin-Alexa Fluor 647 was added apically at 5 min. Time is shown in minutes; bar, 5 μm. (B) Measurement of average fluorescent intensity of albumin-Alexa Fluor 647 within VE-cadherin-GFP junction over time. Fluorescence was normalized to starting fluorescent intensity before addition of albumin-Alexa Fluor 647. (C) Bar graph showing the permeability rate constant from B in endothelial monolayers on gelatin and N-cad-BioS. The permeability rate constant was reduced in cells grown on N-cad-BioS as compared with gelatin.  $n = 14-15$  junctions from three independent experiments. (B) Data are presented as mean  $\pm$  SEM; (C) data are presented as mean  $\pm$  SD; \*,  $P < 0.05$ , a two-tailed, unpaired t test.

side of VE-cadherin junctions (Fig. S3, E and F). In contrast, cells grown on the control substrate gelatin showed little such N-cadherin accumulation (Fig. S3, E and F). Furthermore, ECs grown on N-cad-BioS (but not on inert, denatured N-cad-BioS) showed significantly greater VE-cadherin accumulation as compared with cells grown on gelatin (Fig. 2, D and E; and Fig. S3, H-J). VE-cadherin expression levels were, however, indistinguishable between the groups (Fig. S3 G). Importantly, deficiency in N-cadherin in ECs failed to increase VE-cadherin accumulation in the cells grown on N-cad-BioS (Fig. 2 E and Fig. S3, K-M), indicating the role of N-cadherin-activated signaling in mediating the assembly of VE-cadherin junctions. Furthermore, consistent with the above in vivo endothelial permeability results (Fig. 1, A-D), VE-cadherin junctions that assembled in endothelial monolayers grown on N-cad-BioS in vitro were less permeable to albumin as compared with junctions formed in ECs grown on gelatin (Fig. 3, A-C). This finding reinforced our in vivo observation that defective VE-cadherin junctions in *Cdh2* iEC-KO or iPC-KO mice were associated with increased junctional permeability (Fig. 1, A-D).

To gain insights into the role of N-cadherin-activated signaling in assembling AJs, we next determined the kinetics of VE-cadherin assembly at AJs using the photo-convertible fluorescent probe Dendra2 tagged to the C terminus of VE-cadherin (Fig. 4). Simultaneous imaging of VE-cadherin-Dendra2 at  $\lambda = 488$  and 543 nm after photo-conversion enabled the measurements of both kinetics of VE-cadherin recruitment (trafficking of VE-cadherin to junctions) and VE-cadherin internalization (trafficking of VE-cadherin from junctions; Fig. 4, A-D). We observed that VE-cadherin recruitment and internalization rate constants in ECs grown on gelatin were  $6 \pm 2 \times 10^{-3}$  and  $11 \pm 2 \times$

$10^{-3} \text{ s}^{-1}$ , respectively (Fig. 4, C and E). However, the recruitment rate constant was fourfold greater ( $25 \pm 4 \times 10^{-3} \text{ s}^{-1}$ ) in the cells grown on N-cad-BioS as compared with control (Fig. 4, A-C). In contrast, the rate of VE-cadherin internalization did not change in the cells grown on N-cad-BioS (Fig. 4, A, D, and E). Thus, these results show that N-cadherin activated the signaling pathway responsible for mediating the recruitment of VE-cadherin to AJs.

#### N-cadherin induces assembly of VE-cadherin junctions through activation of the dual Rac1/RhoA GEF Trio

To identify the signaling mechanisms responsible for the N-cadherin-dependent assembly of AJs, we used N-cadherin-coated beads to capture the N-cadherin adhesion complex from primary human pulmonary artery ECs (Fig. S4 A). Mass spectrometry analysis of the N-cadherin adhesion complex identified canonical members of the cadherosome,  $\alpha$ -,  $\beta$ -, and p120-catenins (Fig. S4 B and Table S1). We also identified several actin-binding proteins (Fig. S4, B and C; and Tables S1 and S2) consistent with the known association of the N-cadherin adhesion complex proteins to the actin cytoskeleton (Hatta et al., 1988). Focusing specifically on proteins that may be important in regulating endothelial permeability, we identified by gene ontology (GO) analysis the association of the N-cadherin complex with several relevant signaling pathways (Fig. S4 C and Tables S2 and S3). The N-cadherin complex was associated with the dual Rac1/RhoA GEF Triple functional domain protein (Trio), along with its binding partner, Trio and actin-binding protein (Triobp; Fig. S4, B and C). Trio, known to interact with several cadherin members (Charrasse et al., 2007; Kashef et al., 2009; Timmerman et al., 2015), contains a GEF1 domain that activates Rac1 and a GEF2 domain, which activates RhoA (Debant

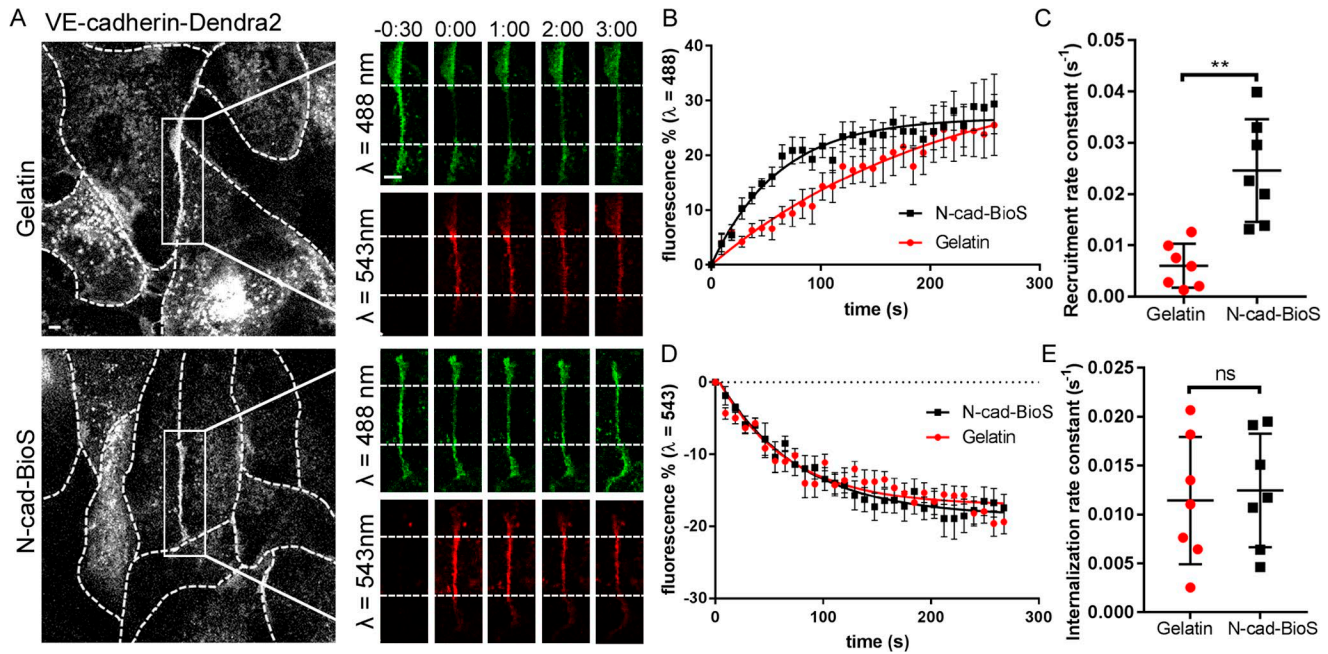


**Figure 4. N-cadherin induces assembly of AJs through increasing the rate of VE-cadherin recruitment. (A)** Time-lapse images of VE-cadherin–Dendra2 before and after photo-conversion at  $t = 0$  within the irradiation zone (indicated by area between dashed lines in insets) in HPAECs grown on either gelatin or N-cad-BioS. 488-nm channel (green) = unconverted VE-cadherin; 543-nm channel (red) = photo-converted VE-cadherin. Dashed lines of grayscale images outline cell borders. Bar, 5  $\mu\text{m}$ ; inset, 2  $\mu\text{m}$ ; time is shown in minutes. **(B and C)** Rate of VE-cadherin recruitment at AJs (B) and recruitment rate constant ( $k$ ) calculated by using nonlinear regression (C) in cells grown on gelatin or N-cad-BioS;  $n = 7$  junctions from three independent experiments. \*\*,  $P < 0.01$ , a two-tailed, unpaired  $t$  test. **(D and E)** Rate of VE-cadherin internalization at AJs (D) and internalization rate constant (E) in cells grown on gelatin or N-cad-BioS;  $n = 7$  junctions from three independent experiments. ns, a two-tailed, unpaired  $t$  test. (B and D) Data are shown as mean  $\pm$  SEM. (C and E) Data are shown as mean  $\pm$  SD.

et al., 1996). We observed that Trio was recruited to the N-cadherin complex formed at the abluminal side rather than interacting directly with N-cadherin (Fig. S4, D–H). Recruitment of Trio to the N-cadherin adhesion complex through the N-terminal portion of Trio (Fig. S4, G and H) was evident biochemically (Fig. S4, D and H) as well as microscopically (Fig. S4, E–G). We also observed that the formation of the N-cadherin adhesion complex had no effect on the association of Trio with VE-cadherin junctions (Fig. S5 A).

We next addressed the role of Trio in assembling VE-cadherin junctions. Trio depletion had no effect on the assembly of VE-cadherin junctions in cells grown on gelatin (Fig. 5, A and B; and Fig. S5 B), whereas Trio depletion significantly reduced the area of VE-cadherin junctions in the cells grown on N-cad-BioS (Fig. 5, A and B); thus, indicating the involvement of Trio in N-cadherin adhesion mediated assembly of VE-cadherin junctions. Furthermore, overexpression of the Trio inactive (“dead”) GEF1 mutant (Trio-D1d) only partially restored VE-cadherin adhesion area in Trio-depleted cells, whereas overexpression of the GEF2 “dead” mutant (Trio-D2d) failed to rescue VE-cadherin adhesion area (Fig. 5 C and Fig. S5 C). However, overexpression of full-length (FL) GFP-Trio in either control or Trio siRNA-depleted cells significantly increased the VE-cadherin adhesion area as compared with cells overexpressing GFP alone (Fig. 5 C). These findings together show that activities of both Trio GEF1 and GEF2 domains downstream of N-cadherin adhesion are required for assembling VE-cadherin junctions.

To reinforce these findings, we next investigated the role of N-cadherin–Trio signaling in regulating the dynamics of VE-cad-

herin at AJs using the Dendra2 probe described in Fig. 4. Loss of Trio significantly reduced the rate constant of VE-cadherin recruitment to AJs to  $4 \pm 10^{-3} \text{ s}^{-1}$  as compared with the value  $26 \pm 5 \times 10^{-3} \text{ s}^{-1}$  observed in control siRNA-treated cells grown on N-cad-BioS (Fig. 5, D–F), whereas this did not occur in endothelial monolayers grown on gelatin (Fig. S5, D and E). Trio knockdown, however, had no effect on the rate of VE-cadherin internalization (Fig. 5, G and H; and Fig. S5, F and G). These data thus demonstrate N-cadherin–Trio signaling is required for the assembly of VE-cadherin junctions.

#### N-cadherin-dependent Rac1 activation via Trio mediates assembly of VE-cadherin junctions

To determine whether N-cadherin–Trio signaling activates Rac1, we precipitated GEFs with a nucleotide-free Rac1 G15A mutant from cells grown on either gelatin or N-cad-BioS (Fig. 6, A and B). We observed increased interaction of Trio with Rac1 G15A in cells grown on N-cad-BioS as compared with gelatin (Fig. 6, A and B), indicating that N-cadherin adhesion promoted the interaction of Rac1 with Trio. Using the fluorescence resonance energy transfer (FRET) Rac1 biosensor (MacNevin et al., 2016), we observed increased Rac1 activity at AJs in ECs grown on N-cad-BioS as compared with gelatin (Fig. 6, C–E). Furthermore, depletion of Trio reduced Rac1 activity at AJs in the cells grown on N-cad-BioS but had no effect on Rac1 activity in cells grown on gelatin (Fig. 6, C–E). These data demonstrate that N-cadherin adhesion activates Trio-dependent Rac1 signaling at VE-cadherin junctions.



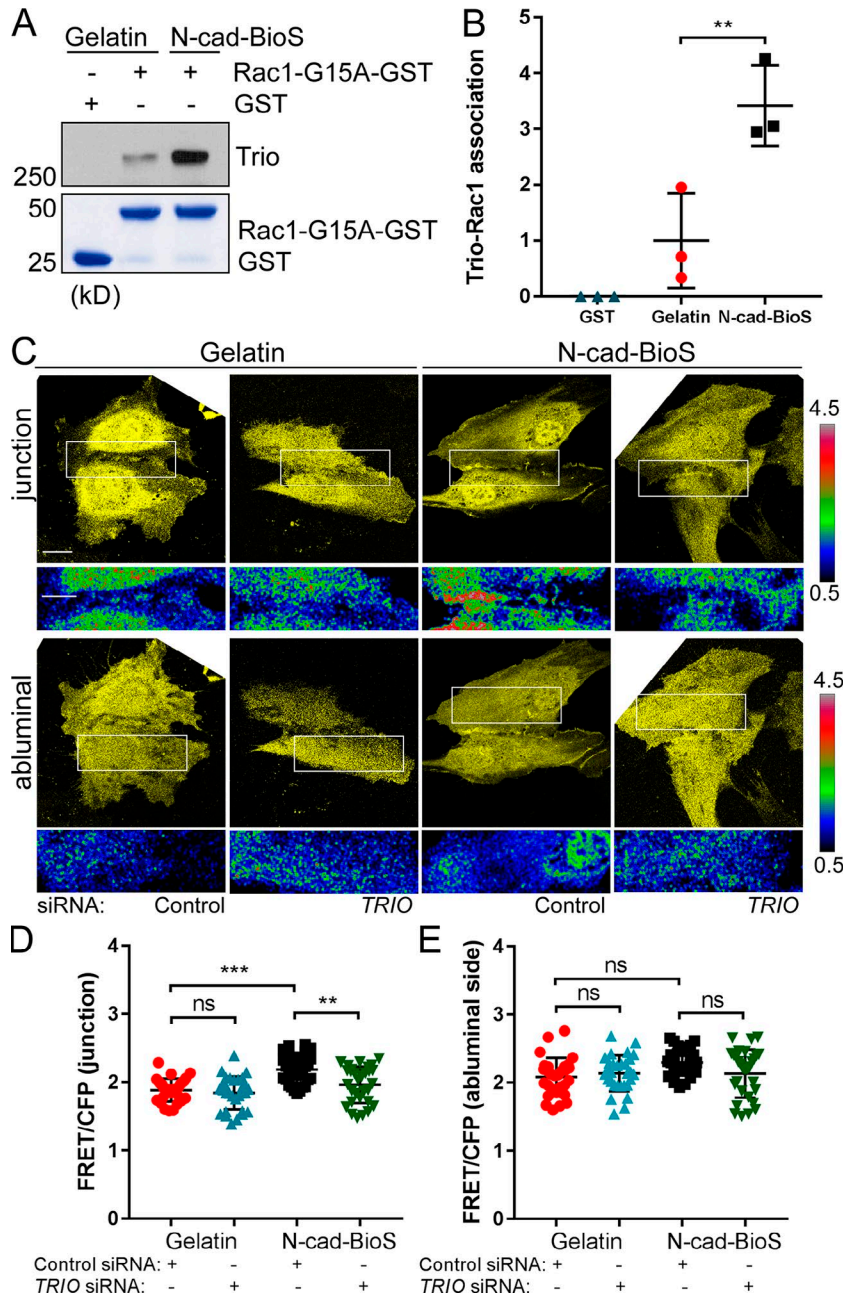


**Figure 6. N-cadherin activates Trio GEF1 mediated Rac1 signaling.** (A) Pull-down of GEFs with GST and GST-Rac1(G15A) from HPAECs grown on gelatin and N-cad-BioS. The resulting precipitates were probed for Trio. Trio and Rac1 interaction increased in cells grown on N-cad-BioS as compared with gelatin. 5% Coomassie-stained proteins used for pull-down. (B) Quantification of Trio GEF1 activity from A. Data are normalized to Trio activity in cells grown on gelatin.  $n = 3$  independent experiments. \*\*,  $P < 0.01$ , ANOVA with Tukey's post hoc test. (C) Confocal images of YFP and Rac1 activity (FRET/CFP) at AJs and abluminal surface of HPAECs grown on either gelatin or N-cad-BioS and treated with control or *TRIO* siRNA. Ratiometric images were scaled from 0.5 to 4.5 and color-coded as indicated on the right. Warmer colors denote higher Rac1 activity. Trio-dependent increase in Rac1 activity is seen at AJs but not at the abluminal surface of the cells grown on N-cad-BioS. Bar, 10  $\mu\text{m}$ . (D and E) Relative Rac1 activity presented as FRET/CFP from images in C;  $n = 20$  junctions or abluminal surfaces from eight cells per group from three independent experiments. \*\*,  $P < 0.01$ ; \*\*\*,  $P < 0.001$ , ANOVA with Tukey's post hoc test. (B, D, and E) Data are shown as mean  $\pm$  SD.

the effects of Trio knockdown in reducing the VE-cadherin recruitment rate to AJs in cells grown on N-cad-BioS (Fig. S6, C–G). Importantly, we observed that photo-activation of PA-Rac1 but not the light-insensitive (LI-Rac1) probe (Wu et al., 2009) restored the defective VE-cadherin recruitment rate in Trio-deficient cells (Fig. 7, A–C) and in cells treated with ITX3 (Fig. S6, H–J). Together, these data demonstrate that formation of the N-cadherin–Trio complex activates Rac1, which in turn signals the assembly of VE-cadherin junctions.

**N-cadherin adhesion-mediated signaling increases Trio-RhoA-dependent intracellular tension to reinforce Rac1 signaling at AJs.**

We next addressed the contribution of the Trio GEF2 domain in mediating the activation of RhoA (Debant et al., 1996) and

whether this also contributed to assembly of VE-cadherin junctions. Here we specifically determined whether RhoA-mediated intracellular tension, which is known to occur at AJs (Acharya et al., 2017), enables the activation of the Trio GEF1 domain, and thus reinforces Rac1-mediated recruitment of VE-cadherin at AJs. Upon measuring RhoA activity in ECs grown on N-cad-BioS, we observed that N-cadherin adhesion increased RhoA activity at the abluminal surface as well as AJs in a Trio-dependent manner (Fig. 8, A–C). Depletion of Trio, however, had no effect on RhoA activity in ECs grown on gelatin (Fig. 8, A–C), indicating the requirement of N-cadherin–Trio signaling in activating RhoA. Furthermore, we observed increased interaction of Trio with the active RhoA G17A mutant in cells grown on N-cad-BioS as compared with gelatin (Fig. 8 D), indicating increased binding of RhoA to Trio.

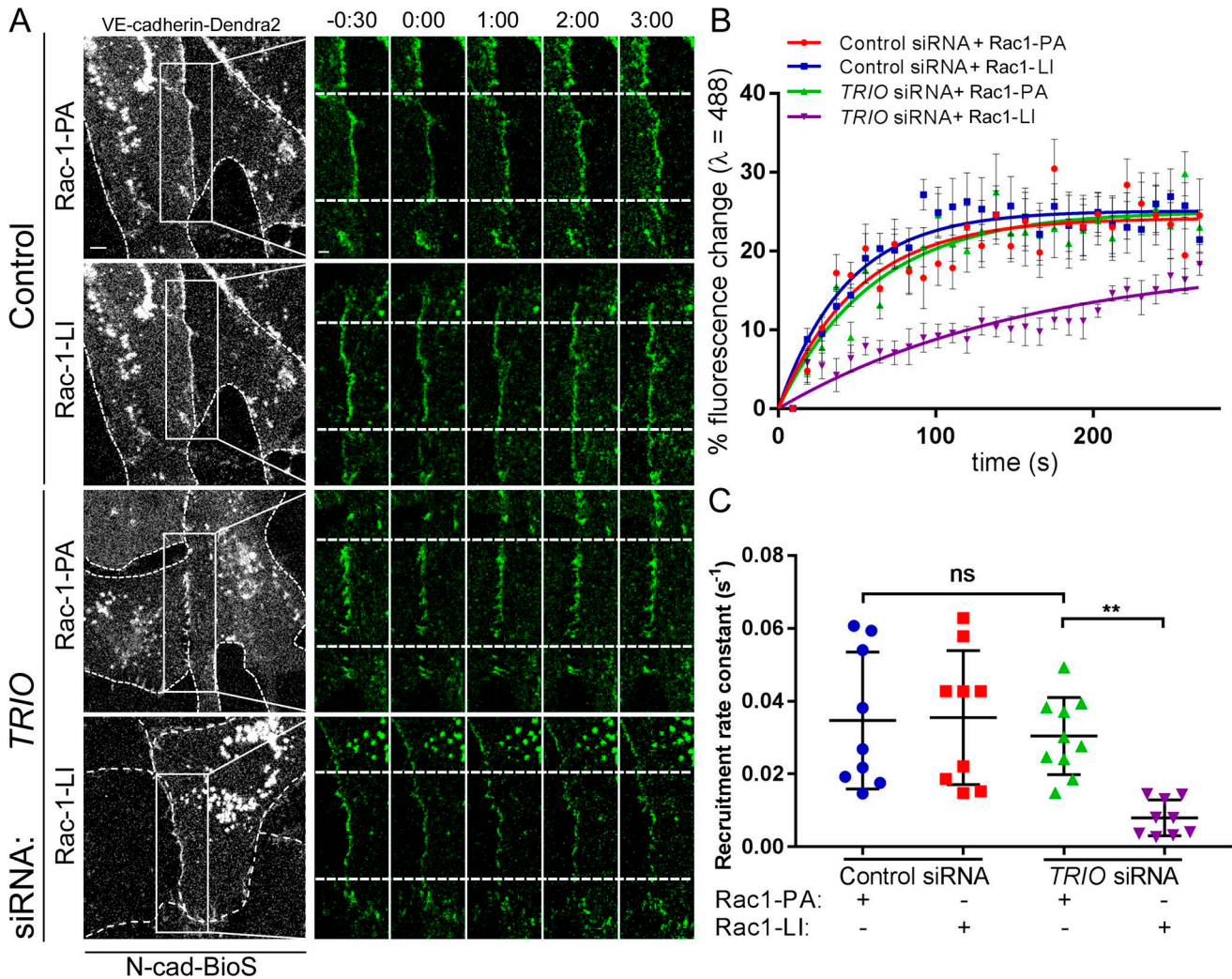


**Figure 7. Photo-activation of Rac1 restores VE-cadherin recruitment in Trio-deficient ECs. (A)** Time-lapse images of VE-cadherin–Dendra2 before and after photo-conversion at  $t = 0$  (as in Fig. 4) in HPAECs grown on N-cad-BioS after siRNA Trio depletion or treatment with control siRNA. CFP–Rac1-photoactivatable (PA) or CFP–Rac1–light-insensitive mutant (LI) were activated within the photo-conversion zone (rectangle) with  $\lambda = 458$  nm. 488-nm channel (green) = unconverted VE-cadherin; 543-nm channel (red) = photo-converted VE-cadherin. Dashed lines of grayscale images outline the cell borders. Photoactivation of PA–Rac1 but not LI–Rac1 rescued the VE-cadherin recruitment rate in Trio-depleted cells. Bar, 5  $\mu$ m; insets, 2  $\mu$ m; time is shown in minutes. **(B and C)** Rate of VE-cadherin recruitment to AJs (B) and recruitment rate constants (C) from data in A;  $n = 7$  junctions from three independent experiments. \*\*,  $P < 0.01$ , ANOVA with Tukey’s post hoc test. (B) Data are shown as mean  $\pm$  SEM. (C) Data are shown as mean  $\pm$  SD.

Next, to investigate the role of RhoA activity in assembling VE-cadherin junctions, we determined alterations in VE-cadherin junctions in cells treated with the Rho kinase inhibitor Rockout (Fig. 9 A). Inhibition of RhoA reduced both phosphorylation of myosin light chain 2 and the VE-cadherin adhesion area of the cells grown on N-cad-BioS but not on gelatin (Fig. 9, B and C). These data suggest that intracellular tension downstream of N-cadherin–Trio–RhoA signaling like Rac1 also contributes to the assembly of VE-cadherin junctions. We next addressed the possible role of RhoA and intracellular tension in activating the Trio GEF1 domain by treating cells either with Rockout or with the myosin light chain 2 inhibitor blebbistatin, which both inhibit intracellular tension (Straight et al., 2003). Both treatments reduced Trio GEF1 activity in the cells grown on the N-cad-BioS platform (Fig. 9, D and E), demonstrating that RhoA-mediated intracellular tension downstream of N-cadherin contributes to

the activation of the Trio–Rac1 pathway, which thereby mediated the recruitment of VE-cadherin to AJs (Fig. 9 F). However, the activation of intracellular tension in cells grown on gelatin failed to increase the VE-cadherin adhesion area (Fig. S7, A–D), demonstrating that tension alone was insufficient to increase VE-cadherin assembly; rather, activation of both RhoA and Rac1 through Trio was required.

## Discussion

This study describes the fundamental role of N-cadherin adhesion, which forms between ECs and pericytes, in signaling the assembly of VE-cadherin junctions and in restricting vascular permeability. This role of N-cadherin involves the formation of the N-cadherin adhesion complex with the dual RhoGEF Trio to activate both Rac1 and RhoA signaling at AJs. We showed that Rac1



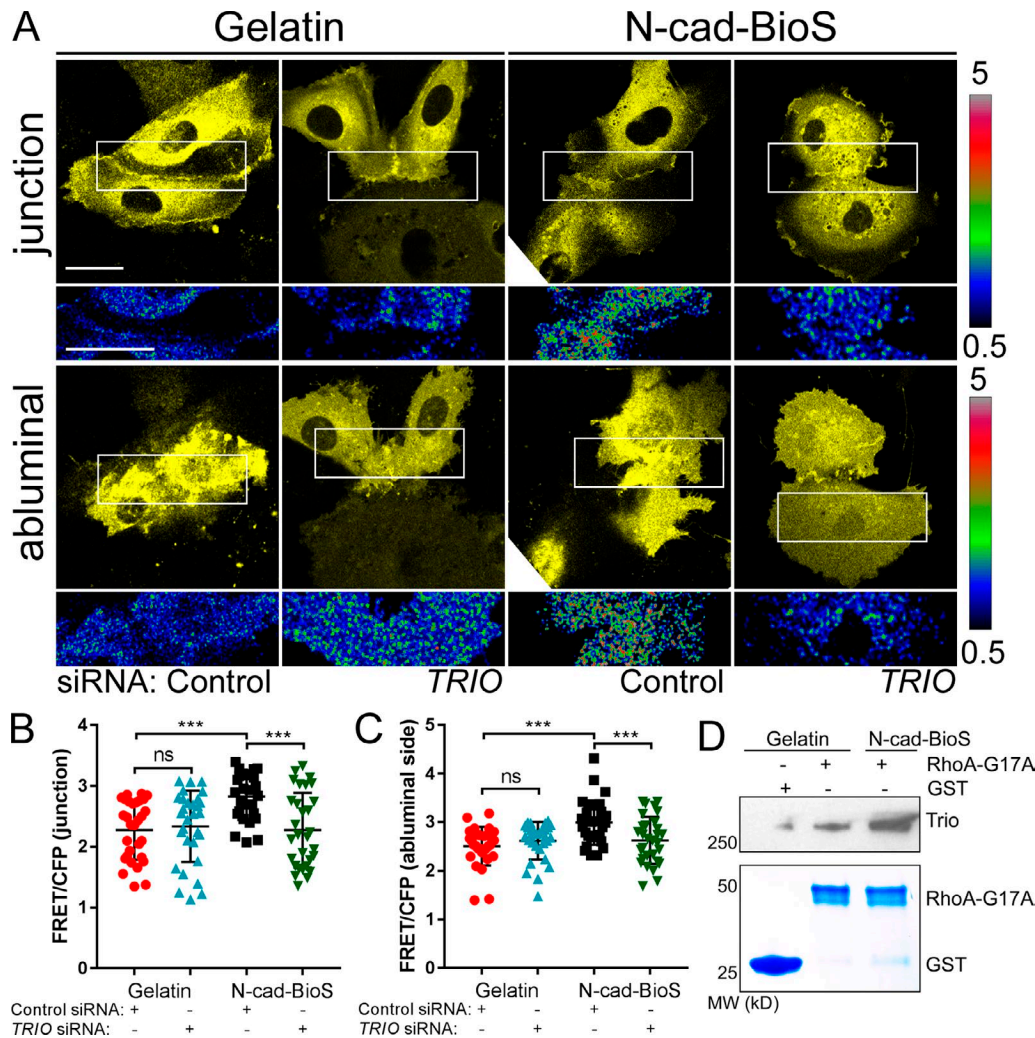


Figure 8. **N-cadherin interaction with Trio activates RhoA.** (A) Confocal images of YFP and RhoA activity (FRET/CFP) at AJs and abluminal surface of HPA ECs grown on either gelatin or N-cad-BioS and treated with control or *TRIO* siRNA. Ratiometric images were scaled from 0.5 to 5 and color-coded as indicated on the right. Warmer colors denote higher RhoA activity. A Trio-dependent increase in RhoA activity is observed at both AJs and abluminal surface of cells grown on N-cad-BioS. Bar, 10  $\mu$ m. (B and C) Relative RhoA activity presented as FRET/CFP ratio at AJs (B) and abluminal surfaces (C) of ECs from images in A;  $n = 20$  junctions or abluminal surfaces from eight cells per group from three independent experiments. \*\*\*,  $P < 0.001$ , ANOVA with Tukey's post hoc test. Data are shown as mean  $\pm$  SD. (D) Pull-down of GEFs with GST and nucleotide free GST-RhoA (G17A) mutant from HPAECs grown on gelatin and N-cad-BioS. The resulting precipitates were probed for Trio. Trio and RhoA interaction increased in cells grown on N-cad-BioS as compared with gelatin. 5% Coomassie-stained proteins used for pull-down.

activation via the Trio GEF1 domain induces the recruitment of VE-cadherin to AJs. RhoA activation by the Trio GEF2 domain increases intracellular tension, and promotes Trio GEF1 domain-dependent activation of Rac1 at AJs to reinforce the assembly of AJs. Thus, Rac1 and RhoA function in a coordinate manner to establish the restrictive nature of the endothelial barrier.

Our studies describe a novel role of N-cadherin adhesion-mediated signaling in ECs and in regulating endothelial permeability. Pericyte coverage of capillaries is organ-specific and varies depending on the tissue type and the organ's endothelial barrier requirement (Armulik et al., 2005). Pericyte numbers are the highest in the brain and retinal capillaries, which also have the lowest permeability values (Armulik et al., 2011). Reduction in pericyte number in *pdgf-b<sup>ret</sup>* allele mice and a microfluidic pericyte-EC co-culture resulted in increased endothelial permeability (Armulik et al., 2010; Daneman et al., 2010; Alimperti

et al., 2017). Also, the loss of pericytes due to activation of inflammatory pathways (Zeng et al., 2016; Alimperti et al., 2017) is implicated in promoting leakiness of capillaries (e.g., in diabetic retinopathy, acute lung injury, septic shock, and brain trauma). Although pericytes appear to have an important role in endothelial permeability regulation, the signaling mechanisms by which they control permeability are not well understood. Since N-cadherin adhesion between ECs and pericytes plays a role in regulating the endothelial barrier in vitro (Alimperti et al., 2017), here we determined the involvement of N-cadherin heterotypic adhesion in regulating microvessel permeability in vivo. Our results show that inducible deletion of *Cdh2* (N-cadherin) in either ECs or pericytes increases junctional permeability of capillaries in lung and brain.

Increased endothelial permeability observed upon deletion of *Cdh2* was associated with dysregulation of VE-cadherin junc-

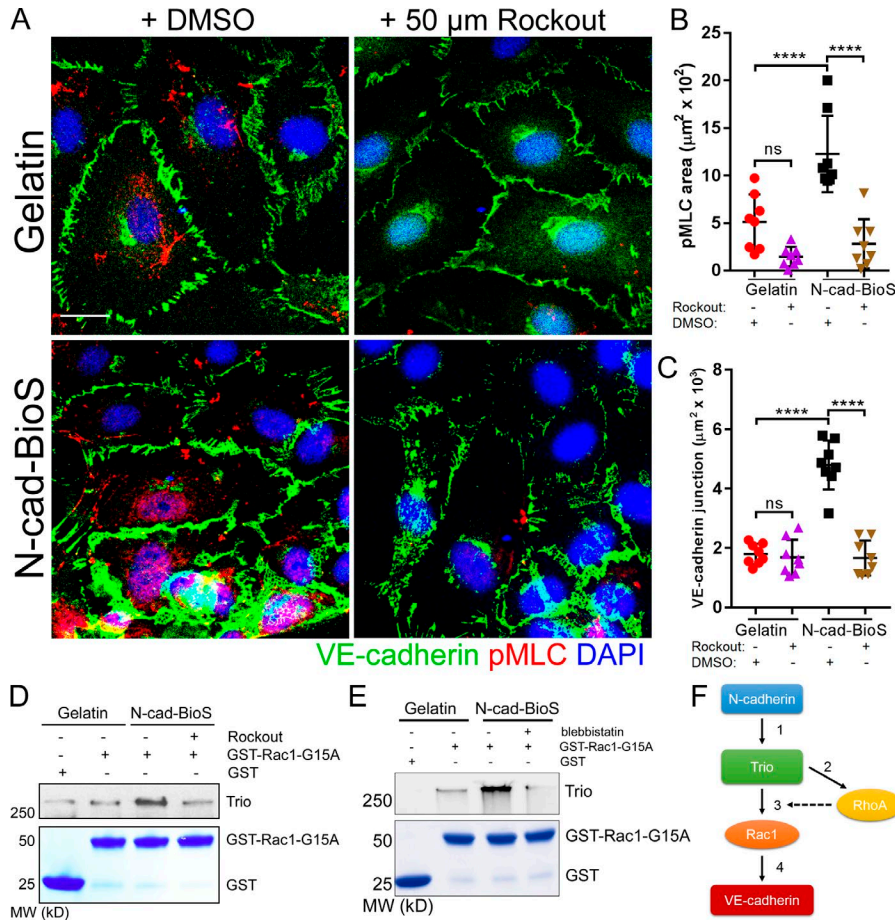


**Figure 9. N-cadherin interaction with Trio increases intracellular tension and reinforces Rac1 activation and promotes assembly of VE-cadherin junctions. (A)** Confocal images of HPAECs grown on either gelatin or N-cad-BioS and treated with 50  $\mu$ M Rockout to inhibit Rho kinase (ROCK) or vehicle (DMSO). Cells were stained for VE-cadherin (green), phosphorylated myosin light chain (pMLC, red) and nuclei (DAPI, blue). Bar, 10  $\mu$ m. **(B and C)** Quantification of phospho-MLC (B) and VE-cadherin junction area (C) from images in A. Inhibition of ROCK significantly reduced the area of VE-cadherin adhesion only in cells grown on N-cad-BioS.  $n = 8$  images per group from three independent experiments. \*\*\*\*,  $P < 0.0001$ , ANOVA with Tukey's post hoc test. Data are shown as mean  $\pm$  SD. **(D)** Analysis of Trio activity. Pulldown of Trio with GST and GST-Rac1(G15A) from HPAECs grown on gelatin and N-cad-BioS platforms after treatment with DMSO (vehicle) or 50  $\mu$ M Rockout for 10 min. The precipitates were probed for Trio. Treatment with Rockout reduced Trio interaction with Rac1. 5% Coomassie-stained proteins used for pulldown. **(E)** Analysis of Trio activity. Pulldown of Trio with GST and GST-Rac1(G15A) from HPAECs grown on gelatin and N-cad-BioS platforms after treatment with DMSO (vehicle) or for 50  $\mu$ M blebbistatin for 10 min. The precipitates were probed for Trio. Treatment with blebbistatin reduced Trio interaction with Rac1. 5% Coomassie-stained proteins used for pulldown. **(F)** The circuit describing the role of N-cadherin adhesion-mediated signaling in assembling of VE-cadherin junctions through Trio-mediated activation of both Rac1 and RhoA. (1) N-cadherin forms a complex with Trio; (2) Trio activates RhoA increasing intracellular tension; (3) increased tension activates the Trio GEF1 domain toward Rac1; and (4) Rac1 increases VE-cadherin recruitment to AJs, whereas RhoA reinforces Rac1-mediated assembly of AJs.

tions, the adhesion complex of AJs regulating endothelial permeability (Lampugnani et al., 1992). We demonstrated by measuring the number of pericytes surrounding ECs of capillaries in *Cdh2* iEC-KO and *Cdh2* iPC-KO mice that this response could not be ascribed to a loss in pericyte coverage. As deletion of N-cadherin did not induce the loss of pericytes, our results suggest that the cells may be held in place through integrin-mediated adhesion to the basement membrane (Courtoy and Boyles, 1983).

Since a key focus of these studies was to define the mechanism of N-cadherin-mediated assembly of VE-cadherin junctions, we performed mass spectrometric analysis of N-cadherin-interacting proteins that may be responsible for restricting junctional permeability. We observed that N-cadherin assembles a complex consisting of the dual GEF Trio at the abluminal endothelial surface. Further, the formation of this complex is coupled to the activation of both Rac1 and RhoA via the Trio GEF1 and GEF2 domains, respectively. Trio interaction with N-cadherin appears to be distinct since VE-cadherin interaction with Trio only activates Rac1 (Timmerman et al., 2015).

Previous studies show that cadherin proteins can both positively and negatively regulate Trio activity (Debant et al., 1996;

Seipel et al., 1999; Medley et al., 2003; van Rijssel et al., 2012). VE-cadherin in ECs (Timmerman et al., 2015) and M-cadherin in myoblasts (Charrasse et al., 2002) preferentially activate the Trio GEF1 domain, leading to Rac1 signaling, whereas E-cadherin in epithelial cells inhibited Trio activity through interacting with Triobp (Seipel et al., 2001; Yano et al., 2011). In neural crest cells, cadherin-11 activates both Trio GEF1 and GEF2 domains during development (Kashef et al., 2009). In the present study, we also demonstrate that N-cadherin activates both Rac1 and RhoA via Trio in ECs and that activation of both GTPases is crucial in mediating the assembly of VE-cadherin junctions. The reasons for varying RhoGTPase activation responses induced by the interaction of different cadherins with Trio are unknown. Our data indicate that N-cadherin interaction with Trio activates both Rac1 and RhoA, which is essential for the assembly of VE-cadherin junctions. Whereas Rac1 promotes recruitment of VE-cadherin to AJs, the Trio GEF2 domain activates RhoA, leading to intracellular tension via myosin-II, which in turn reinforces GEF1-dependent Rac1 activation and thus also contributes to the assembly of VE-cadherin junctions. It is not known, however, how RhoA-mediated intracellular tension can activate the interaction

of Rac1 and Trio. RhoA-mediated tension may cause a conformational change to Trio, leading to binding of the GEF1 domain to Rac1 and activation of Rac1 signaling. An analogous process of tension-induced conformational changes also regulates GEF-H1 and GEF p115 activities (Scott et al., 2016).

Aspects of N-cadherin adhesion-mediated signaling through the actin cytoskeleton have been studied in non-ECs (Mary et al., 2002; Comunale et al., 2007; Cosgrove et al., 2016). N-cadherin adhesion in myoblasts induces reorganization of the actin cytoskeleton, leading to myosin-II-dependent maturation of N-cadherin adhesion (Yano et al., 2004; Comunale et al., 2007). This involves recruitment of  $\alpha$ -catenin to nascent N-cadherin adhesion sites and consequent attachment of the adhesion complex to the actin cytoskeleton (Leonard et al., 2011). N-cadherin adhesion also activates Rac1 signaling in fibroblasts and mesenchymal stem cells, which restrains cell contractility and modulates the cell's adaptive response to stiffening of the extracellular matrix (Cosgrove et al., 2016; Alimperti et al., 2017). Our finding that N-cadherin interaction with Trio can activate Rac1 in a tension-dependent manner is consistent with this general concept.

The present results show a key role of small RhoGTPase signaling in regulating permeability of the endothelial barrier through organizing AJs and the actin cytoskeleton (Komarova et al., 2017). We demonstrated that N-cadherin adhesion-mediated signaling promotes the recruitment of VE-cadherin to AJs. These results thus position the N-cadherin-Trio complex as a regulator of Rac1 and RhoA activities and the assembly of VE-cadherin junctions. Rac1 is a reversible modulator of intracellular tension that enables the stabilization of VE-cadherin trans-interactions to form mature AJs (Daneshjou et al., 2015). Rac1 functions by reducing the rate of VE-cadherin internalization from AJs and thus induces assembly of AJs (Daneshjou et al., 2015). These results explain Rac1-dependent reannealing of AJs in response to endothelial barrier-enhancing mediators such as sphingosine-1-phosphate (Paik et al., 2004; Itoh et al., 2012). Our present observations extend these findings by defining the role of N-cadherin adhesion as a mechanism responsible for establishing a restrictive endothelial barrier through N-cadherin-mediated activation of the RhoGEF Trio. In our model described in Fig. 9 F, N-cadherin-mediated activation of Rac1 via Trio GEF1 and activation of RhoA via GEF2 coordinate the assembly of VE-cadherin junctions. RhoA functions by increasing intracellular tension, which facilitates Trio GEF1-dependent activation of Rac1 to reinforce the recruitment of VE-cadherin to AJs. In this model, Rac1 is ultimately responsible for the assembly of VE-cadherin junctions and restricting endothelial permeability (Fig. 9 F). Based on our results, RhoA-mediated tension alone is insufficient to increase VE-cadherin assembly, suggesting that both RhoA and Rac1 activation mediated by the interaction of N-cadherin with Trio is needed to form a restrictive endothelial barrier. Consistent with our model, defective VE-cadherin junctions in Trio-deficient ECs are rescued by activating Rac1 at AJs using a photoactivable probe.

Our findings demonstrate a novel role for N-cadherin-Trio signaling in cooperatively activating both RhoA and Rac1 and thereby assembling VE-cadherin junctions. Because the level of VE-cadherin expression and complexity of VE-cadherin junctions

at AJs are correlated with the permeability value of AJs (Lampugnani et al., 1992), our study provides direct mechanistic support for this relationship. Specifically, N-cadherin interaction with Trio is an important mechanism in the assembly of VE-cadherin junctions and thus endothelial permeability. It is possible that the specialized differences in N-cadherin-Trio complex interactions are responsible for the differential permeability values in different vascular beds (e.g., blood-brain barrier versus other endothelial barriers; Armulik et al., 2010). Our results also raise the possibility that endothelial AJs in capillaries can be strengthened through promoting N-cadherin-Trio interactions such that AJs become more resistant to mechanical forces such as high hydrostatic pressure or shear stress (Weisberg, 1978; Baeyens et al., 2016). The understanding of N-cadherin mechanobiology may thus lead to therapeutic strategies that limit vascular leakage in inflammatory diseases.

## Materials and methods

### Experimental model and subject details

#### Reagents

A full list of reagents can be found in Table S4.

#### Mice

All mice were maintained on a C57BL/6 genetic background. Deletion of the *Cdh2* gene in ECs and pericytes, herein *Cdh2* iEC-KO and *Cdh2* iPC-KO mice, was generated by crossing loxP-flanked *Cdh2* (*Cdh2*<sup>fllox/fllox</sup>) mice (Luo and Radice, 2005) with either end-SCL-Cre-ER<sup>T</sup> (Gu et al., 1994; Göthert et al., 2004) or PDGFR $\beta$ -P2A-CreER<sup>T2</sup> transgenic mice, respectively (Cuervo et al., 2017). *Cdh2*<sup>fllox/fllox</sup> mice have been bred to the F10 generation, authenticated by genotyping and Western blotting for N-cadherin expression in lung ECs. No change in the expression of N-cadherin was observed in *Cdh2*<sup>fllox/fllox</sup> as assessed by Western blotting analysis of endothelial-specific fractions or isolated pericytes. *Cdh2* iEC-KO and *Cdh2* iPC-KO mice demonstrate no gross change in either behavior or health. *Cdh2*<sup>fllox/fllox</sup> littermates were used as control (denoted Cre<sup>-</sup>). Both male and female mice were used in this study. Littermates were randomly assigned to experimental groups.

All animals were housed in the animal facility at the University of Illinois at Chicago, where they were maintained in a 12-h light/12-h dark cycle environment with access to water and food. All proposed animal procedures and experiments were approved by the University of Illinois at Chicago Animal Care and Use Committee. All animal studies were performed under the auspices of the University of Illinois Animal Care and Use Committee.

Tamoxifen (T6548; Sigma-Aldrich) was reconstituted in 1 ml corn oil (C8267; Sigma-Aldrich) at a concentration of 20  $\mu$ g/ml. The solution was passed through a 0.2- $\mu$ m filter and used fresh at 2  $\mu$ g/mouse. Tamoxifen was injected for five consecutive days in 6–8-wk-old mice to delete *Cdh2* in endothelial or mural cells. Mice were used for experiments at different times after Cre induction (2–6 wk after induction for permeability studies, pericyte analysis, Western blotting, and VE-cadherin analysis; 36–40 wk for pericyte analysis in aged *Cdh2* iEC-KO mice). Deletion of *Cdh2* in either cell type is not lethal and causes no major health issue even 1 yr after induction.

The sample size was calculated for each experiment using power analysis using JMP release 6 software programs (SAS).

**Permeability times surface area product.** Given a mean value of  $6.8 \pm 0.8 \mu\text{l}/\text{min}/100$  dry lung in *Mus/Cdh2<sup>flox/flox</sup>* mice, a population SD of 8, a significance level of 0.05, and power of 0.8 requires a group size of  $n = 9$  as the minimum number of mice required to obtain a significant increase of 50% more than the control. Since the differences between groups were about two-fold, we limited our animal studies to five to eight mice per group, required to reach statistical significance.

**Lung and brain tissue (histology).** We used at least three mice per experiment due to variability of the effect of *Cdh2* deletion. We generated at least five sections for each analysis by immunofluorescent staining.

**Lung lysate collection.** Lung lysate collection was performed as described by our group (Komarova et al., 2012). To collect endothelial fractions directly from lungs of *Cre*<sup>-</sup> or *iEC*-KO mice, mice were anesthetized and lungs were perfused with Hepes-buffered RPMI medium (pH 7.4) through the pulmonary artery at constant flow (0.4 ml/min), temperature (37°C), and venous pressure (~0 cm H<sub>2</sub>O) with continued ventilation (120/min, peak inspiratory pressure of 10 cm H<sub>2</sub>O, end expiratory pressure of 2 cm H<sub>2</sub>O). The endothelial lysates were collected via a left atrial cannula by perfusing fractionation buffer (50 mM Tris-Cl, pH 7.8, 0.2% Triton X-100, and protease and phosphatase inhibitor cocktails). Samples were collected every 30 s. Fractions positive for endothelial-specific markers were used for analysis of N-cadherin, VE-cadherin, p120 catenin, and tubulin.

**Cell isolation.** One mouse gives  $\sim 2.5 \times 10^5$  ECs after several days of culture and reseeded for an experiment. We used three to five mice per group to pool the cells for each individual experiment.

All the experiments involving animals have had two or more independent replications.

### Human primary ECs

Human pulmonary aortic ECs (CC-2530; Lonza) and human lung microvascular ECs (CC-2527; Lonza) were grown in Endothelial Basal Media (CC-3156; Lonza) supplemented with Endothelial Growth Medium 2 (CC-4176; Lonza) or Endothelial Growth Medium 2 MV (CC-4147; Lonza), respectively, and supplemented with 10% FBS (35-015-CVX; Mediatech). Cells were used at passages four to eight. All cell lines were maintained at 37°C and 5% CO<sub>2</sub>.

### Primary murine lung microvascular ECs

The isolation and culture of microvascular ECs from mouse lungs were performed as described by us (Siddiqui et al., 2011). Briefly, lungs were removed, minced, and suspended in 1.0 mg/ml collagenase A. The released cells were centrifuged, resuspended, and filtered through a 200- $\mu\text{m}$  mesh filter. Platelet-EC adhesion molecule (PECAM)-1-positive cells bound to Dynabeads M-450 were separated on a magnetic column and grown in EGM-2 MV (CC-3202; Lonza) culture medium supplemented with 15% FBS (35-015-CVX; Mediatech). KO of specific genes was validated with Western blot analysis. Characterization of ECs was routinely assessed by measuring Dil-Ac-LDL uptake and by immunostaining for endothelial-specific markers, VE-cadherin, von Willebrand factor, and lectins as standardized for primary culture.

### Isolation of primary pericytes

Cortical pericytes were isolated as described (Boroujerdi et al., 2014) with modification. Briefly, the cortex was dissected, chopped, and centrifuged in Minimal Essential Media MEM $\alpha$  (Thermo Fisher Scientific) at 1,000 g for 5 min at 4°C. The pellet was triturated using a 19-G needle in MEM $\alpha$  containing papain (17 U per brain; Worthington Biochemical) and DNase (84 U per brain; Worthington Biochemical). The suspension was then incubated for 15 min in a 37°C water bath, triturated with a 21-G needle, and mixed with 2 volumes of a 25% BSA solution and centrifuged at 3,880 g for 15 min at 4°C. The pellet was suspended in pericyte media (1231; ScienCell) containing pericyte growth supplement (1252; ScienCell), 10% FBS, penicillin/streptomycin, and heparin (5.5 U per 1 ml), and centrifuged at 1,000 g for 5 min at 4°C. The pericytes were grown in pericyte media on plates coated with 50  $\mu\text{g}/\text{ml}$  fibronectin (F0895; Sigma-Aldrich), 0.0001% laminin (L2020; Sigma-Aldrich), and 0.005% collagen type 1 (C8919; Sigma-Aldrich). Cells were used at P2 for Western blot analysis.

### Methods details

#### <sup>125</sup>I-albumin permeability assay

150  $\mu\text{l}$  of <sup>125</sup>I-albumin containing 2  $\mu\text{Ci}$  was intravenously injected via tail vein. 30 min later, mice were anesthetized with 2.5% isoflurane (Pinter et al., 1974). The depth of anesthesia was determined by pinching the toe of the animal. Blood and organs (lung and brain) were collected for measurement of radioactivity in the whole organ using a gamma counter. Humane euthanasia was performed by vital organ removal under anesthesia.

#### Fluorescent dextran tracers

10-kD and 70-kD dextran tracers conjugated with Alexa Fluor 555 or Oregon Green 488 (1 mg/mouse) were injected intravenously via retroorbital sinus (100  $\mu\text{l}$  per mouse). Dextran tracers were chosen to measure leakage only through the paracellular pathway (Kawedia et al., 2007) and confirmed opening of inter-endothelial junctions (as compared with albumin, which can be transported through caveolae-mediated transcytosis). The mouse was euthanized with 2.5% isoflurane and placed in a supine position, and anesthesia was continued by a nose cone. Heparin sodium (700 U/kg) was administered intraperitoneally to prevent clotting. The whole body was perfused through the right ventricle to remove intravascular dye with warm PBS, and the right atrium was removed to allow clearance. Lung and brain tissues were collected, fixed, embedded, and sectioned. The samples were analyzed using a confocal LSM880 microscope, and leak of fluorescent dextran outside of circulation was quantified as described below.

#### Tissue fixation and freezing for cryosectioning

The whole body was perfused through the right ventricle to remove intravascular dye and with warm PBS to remove blood, and either prefixed in situ by perfusing 4% formaldehyde or embedded in optimal cutting temperature compound and frozen in block. The lung was inflated before fixation or optimal cutting temperature compound embedding. The frozen tissue (brain or lung) was cryosectioned. 12- $\mu\text{m}$  sections were sliced, attached to a coverslip, and fixed in 4% formaldehyde overnight. Antigen

retrieval was performed by boiling samples in sodium citrate (pH 6.0) for 30 min using a 100°C water bath and stained.

### Immunofluorescent staining

Cells or frozen tissue sections were fixed in 4% formaldehyde for 20 min, washed once with PBS, and permeabilized for 15 min using 0.01% Triton X-100 in PBS. Nonspecific sites were blocked using 3% BSA for 2 h at room temperature. Samples were incubated with primary antibodies using a 1:100 dilution at either 1 h at room temp or overnight at 4°C. Samples were incubated with secondary antibodies using a 1:100 dilution for 1 h at room temperature.

### N-cad-BioS

Glass coverslips or dishes were sonicated for 20 min for each treatment in absolute ethanol, acetone, 2 N HCl, and 10 N sodium hydroxide followed by washing three times with ddH<sub>2</sub>O after each treatment, and allowed to dry completely. Glass coverslips or dishes were incubated overnight in toluene vapor containing 2% Glymo, washed three times in ddH<sub>2</sub>O, and incubated overnight in 2% AB-NTA (Dojindo) at 60°C and 10 mM NiCl<sub>2</sub> and 5 mM glycine (pH 8.0) for 2 h followed by washing three times in ddH<sub>2</sub>O. To attach protein, Ni-NTA surfaces were incubated for 1 h at room temperature with the extracellular domain of N-cadherin fused with a His tag at the C terminus. Protein was covalently linked to the Ni-NTA glass using 50 mM 1-ethyl-3-(3-dimethylaminopropyl)carbodiimide (EDC) and 100 mM n-hydroxysuccinimide (NHS) in 20 mM Hepes and 100 mM NaCl for 45 min at room temperature. Non-covalently linked proteins were eluted by adding 1 M imidazole in 10 mM EDTA (Chevalier et al., 2010). For control surfaces, Ni-NTA surfaces were incubated with 0.2% gelatin and 0.1% fibronectin for 30 min and washed with 20 mM Hepes, 100 mM NaCl, and 1 M imidazole in 10 mM EDTA. Surfaces were denatured using 8 M urea for 30 min.

### Microscopy

Live cell microscopy was performed with a Zeiss LSM 710 confocal microscope equipped with a Zeiss 63× Plan Apochromat 1.4 NA objective and Zeiss Zen software. ECs grown in glass-bottom dishes were imaged at 5% CO<sub>2</sub> and 37°C in phenol-red free Endothelial Growth Medium containing 10% BSA.

Imaging of fixed cells and/or tissue was performed at room temperature with a Zeiss LSM 880 confocal microscope, Zeiss 63× Plan Apochromat, 1.4 NA objective, and Zeiss Zen software unless otherwise specified.

### Live cell imaging of fluorescent albumin permeation across VE-cadherin junctions

Live cells expressing VE-cadherin-GFP were grown on either N-cad-BioS or gelatin-coated surfaces for 24 h to form a confluent monolayer. Alexa Fluor 647-conjugated albumin was added to the cells at a concentration of 1 mg/ml during image acquisition. A z-stack of images was acquired using a Zeiss LSM 710 confocal microscope as described above at 5% CO<sub>2</sub> and 37°C at  $\lambda = 488$  nm (VE-cadherin) and  $\lambda = 647$  nm (albumin) for 30 min.

### Imaging of VE-cadherin dynamics at AJs using VE-cadherin-Dendra2

Live cells expressing the photo-convertible protein VE-cadherin-Dendra2 alone or coexpressing PA-Rac1-mCerulean or LI-Rac1-CFP were imaged at 5% CO<sub>2</sub> and 37°C with  $\lambda = 488$  nm and  $\lambda = 543$  nm for green and red states of Dendra2, respectively, and  $\lambda = 458$  nm for CFP detection. Dendra2 was irreversibly photo-converted from green to red with  $\lambda = 405$ -nm laser at 8–12% power. PA-Rac1 was photoactivated continuously using a 458-nm laser at 8–12% power. Images in green and red channels were simultaneously acquired every 10 s using a Zeiss LSM 710 confocal microscope equipped with two gallium arsenide phosphide detectors, allowing a simultaneous imaging of green and red states of Dendra2 as described by us (Daneshjou et al., 2015). See Quantification and statistical analysis below for further details.

### FRET imaging

Live cells were imaged with a Zeiss LSM 710 confocal microscope at 5% CO<sub>2</sub> and 37°C as described previously (Siddiqui et al., 2011; Daneshjou et al., 2015). Cells were irradiated with a  $\lambda = 458$ -nm laser, and simultaneous FRET and CFP images were acquired at  $\lambda = 570$  nm and  $\lambda = 485$  nm, respectively. A YFP image was acquired separately and used for generation of a binary mask.

### TIRF and epifluorescence imaging of N-cadherin adhesion

Epifluorescent and TIRF images of ECs stained for VE- and N-cadherin proteins were acquired using a Zeiss Axio Observer Z1/7 equipped with an  $\alpha$  Plan-Fluar 100×/1.45 Oil objective, a Hamamatsu CCD camera, and a TIRF adaptor.

### Western blot

Total protein concentrations for each sample were measured using a BCA protein assay kit and were adjusted according to the protein concentration in each sample. Samples were boiled in Laemmli sample buffer for 5 min and separated using the SDS-PAGE system. Proteins were transferred to nitrocellulose membranes overnight at 4°, and nonspecific sites were blocked with 3% milk for 1 h. Proteins of interest were then detected by probing with the indicated primary and horseradish peroxidase-conjugated secondary antibodies, and the immune reactivity was developed using the ECL method.

### Isolation of N-cadherin complexes

N-cadherin-His protein was incubated with magnetic Ni-NTA beads (88831; Thermo Fisher Scientific) at a concentration of 1  $\mu$ g/ $\mu$ l for 1 h at room temperature. N-cadherin-His protein was cross-linked to beads using EDC/NHS for 45 min at room temperature (Chevalier et al., 2010). Beads were incubated with the culture of ECs for 1 h. Proteins were cross-linked with the reversible cross-linker 50  $\mu$ M DTSP. Beads were then collected from cell lysates using a magnetic separator, washed five times in PBS, and boiled in sample buffer containing 1 mM DTT to break the cross-link. Lysates were separated by SDS-PAGE and silver-stained to highlight the bands of interest. Each lane of the gel was cut into three pieces and submitted to the Taplin Biological Mass Spectrometry Facility, Harvard University, Boston, MA,

for analysis by microcapillary liquid chromatography–tandem mass spectrometry.

#### **Purification of GST or GST-Rac1-G15A:**

Transformed DH5 $\alpha$  *Escherichia coli* carrying either GST-Rac1-G15A or GST cDNA were grown overnight. Protein expression was induced with IPTG to a final concentration of 100  $\mu$ M and grown overnight. All the following steps were performed at 4°C. Bacteria was spun down, resuspended in lysis buffer, and sonicated for 1 min. Lysates were then spun down at 20,000 *g* for 15 min. The supernatant was transferred to a tube containing 500  $\mu$ l of glutathione-sepharose preequilibrated in lysis buffer. The tube was rotated at 4°C for 1 h. Beads were spun down and washed twice with 10 ml lysis buffer and then two times with 10 ml HBSS containing 5 mM MgCl<sub>2</sub> and 1 mM DTT. Wash buffer was aspirated to reduce initial sepharose volume of 50% slurry, and 0.5 volumes of glycerol were added. Protein concentration was estimated on Coomassie blue-stained gel and using a series of BSA concentrations as the standard (García-Mata et al., 2006).

#### **Pulldown of Trio with nucleotide-free Rac1 and RhoA**

Cells grown on either gelatin or N-cad-BioS-coated surfaces were washed with PBS and lysed in radioimmunoprecipitation assay buffer. Cells were treated with either 50  $\mu$ M Rockout or blebbistatin for 10 min where indicated. Lysates were collected, and debris was spun down at 16,000 *g* for 1 min. Protein concentration was calculated using a BCA protein assay kit, and the total amount of protein as well as the total volume of each sample were equalized. The lysates were incubated with 10  $\mu$ g GST, GST-Rac1-G15A beads, or RhoA-G17A beads, and rotated for 1 h at 4°C. Beads were then washed six times using lysis buffer. Samples were then boiled in Laemmli buffer at 95°C for 5 min and separated by SDS-PAGE. Proteins were transferred to a nitrocellulose membrane overnight at 4°C and probed with the appropriate antibodies (García-Mata et al., 2006).

#### **Treatment with siRNA and inhibitors**

ECs grown to 70% confluence were treated with scrambled siRNA duplexes or siRNA targeting a specific protein of interest using GeneSilencer (Gentlantis) according to the manufacturer's instructions. Cells were used for the experiments 48–72 h after treatment. Depletion of the target protein was validated by Western blot analysis.

Cells were treated for 30 min with 50  $\mu$ M ITX3 (Bouquier et al., 2009), 50  $\mu$ M Rockout (Yarrow et al., 2005), or 50  $\mu$ M blebbistatin (Straight et al., 2003) for 10 min and used for the experiments. 0.005% DMSO (vehicle) was added to a control group.

#### **Transfection**

Cells were electroporated using the Nucleofector Kits for Primary Cells (Lonza) according to the manufacturer's instructions.

#### **Quantification and statistical analysis**

##### **Image quantification and presentation**

All image quantification (fibrinogen leakage, adhesion area or projected area, VE-cadherin/vessel area, endothelial permeability to albumin, VE-cadherin Dendra2 rates, pericyte coverage,

and FRET/CFP ratios) was performed using ImageJ software except where otherwise noted. GraphPad Prism was used to make all graphs.

#### **Quantification of leakage of fluorescent dextran tracers**

Mouse lung or brain tissues from mice injected with 10-kD and 70-kD dextran tracers were sectioned and imaged using a Zeiss LSM 880 confocal microscope. The far-red channel was used to capture tissue autofluorescence and to measure the total tissue volume. The sections were reconstructed using Imaris software (Bitplane), and the volumes of both tracers and the tissue volume were measured. The data are presented as a ratio of tracer volume to tissue volume.

#### **Quantification of fibrinogen leakage in lung**

To analyze fibrinogen leakage, murine lung sections were immunostained for fibrinogen and CD31. The Z projection of the images was then thresholded to eliminate background fluorescence. The leakage was expressed as the percentage of fibrinogen-positive area normalized to the total vessel area, as previously described (Chang et al., 2017).

#### **Quantification of adhesion area or projected area**

Area was calculated by creating a Z-projected image for each channel using only the in-focus frames of a z-stack. A threshold was used to eliminate background or nonspecific intracellular fluorescence, and the total area of cell or adhesion area between adjacent cells was measured using Metamorph (Daneshjou et al., 2015).

#### **Quantification of VE-cadherin/vessel area**

VE-cadherin/vessel area in lung and brain was calculated by creating a z-projected image for each VE-cadherin and PECAM1 channel. A threshold was used to eliminate background or nonspecific intracellular fluorescence, and the total area of PECAM1 was measured. To determine the VE-cadherin ratio, a binary mask of the PECAM1 image was multiplied by the VE-cadherin image, and the area of VE-cadherin within AJs was measured.

#### **Quantification of VE-cadherin junction area at AJs**

To analyze the amount of VE-cadherin at AJs (defined as an 8-pixel-wide band around the inner edge of the cell) in cells expressing GFP, Trio-GFP, or Trio mutants, a VE-cadherin z-projected image was thresholded to eliminate background fluorescence. The threshold area within an 8-pixel-wide band around the inner edge of the cell was calculated. The data were normalized to cells treated with control siRNA and expressing GFP.

#### **Quantification of endothelial permeability to albumin**

To analyze endothelial permeability to albumin, the average fluorescent intensity of Alexa Fluor 647 was measured in an x-z cross-sectional plane along the VE-cadherin junction. The albumin signal was normalized to the background fluorescence (before albumin was added). The values were plotted as the normalized albumin signal over time. The permeability rate constant (*k*) was calculated by fitting the data to a nonlinear one-phase association equation (Quadri et al., 2012).

### Measurement of VE-cadherin recruitment and internalization rates at AJs using VE-cadherin–Dendra2

VE-cadherin undergoes turnover at junctions through recruitment (influx of new VE-cadherin to the junctions) as well as internalization (efflux of VE-cadherin from the junctions). We measured both the recruitment and the internalization rates of VE-cadherin using the photo-convertible probe Dendra2 tagged to the C terminus of VE-cadherin. Upon irradiation with a 405-nm laser in a specific photo-conversion zone (a 5–10- $\mu$ m section of VE-cadherin junction), the probe changes its emission (irreversibly) from green ( $\lambda = 488$  nm) to red ( $\lambda = 543$  nm), allowing two separate groups of VE-cadherin to be tracked over time. The changes in mean fluorescent intensities at  $\lambda = 488$ -nm and 543-nm maximum emission spectra were measured inside the photo-conversion zone. By measuring the changes in fluorescence of the green channel over time within the irradiation zone, we determined the recruitment of new VE-cadherin to AJs since all VE-cadherin molecules within this zone were photo-converted to red. By measuring the changes in fluorescence of the red channel over time, we determined the internalization of junctional VE-cadherin. For each time point, the relative changes in fluorescence for either green or red were calculated within the irradiation zone. The rate constants for VE-cadherin internalization and recruitment were calculated from decay and recovery kinetics, respectively. The recruitment and internalization rate constants ( $k$ ) were calculated using nonlinear regression to fit the values to the one-phase association equation  $Y = Y_0 + (\text{Plateau} - Y_0) \times [1 - \exp(-k * t)]$ , where  $Y$  = fluorescent intensity,  $Y_0$  = initial fluorescent intensity, Plateau is the maximum or minimum fluorescent intensity (recovery or decay) after photo-conversion, and  $t$  = time (Daneshjou et al., 2015). The rate of VE-cadherin–Dendra2 lateral movement within the cell–cell junction was determined from the rate of fluorescence lateral movement at  $\lambda = 543$  nm outside the photo-conversion zone using kymograph analyses.

### Analysis of N-cadherin complexes

Non-unique peptides were excluded from the mass spectrometry data. 1,120 unique candidates for constituents of N-cadherin complexes were represented by more than 3 of the 20,607 remaining unique peptides or with arbitrarily chosen log<sub>10</sub> mean peptide intensities greater than 6. These candidate proteins were evaluated for known interactions within ten protein interaction databases, including BioGRID, Bell09, HPRD, IntAct, and MINT, as well as other studies via the Human Integrated Protein-Protein Interaction Reference (HIPPIE). Protein interactions were filtered to only include those with confidence scores greater than 0.2 (Alanis-Lobato et al., 2017). Of the 1,120 interrogated proteins, 1,046 had at least two established interactions, with a maximum of 1,759 (IQGAP1) and median of 77 interactions per protein. An interaction profile was created for each of these proteins using a Euclidean distance comparison with all other protein interaction confidence scores.

We chose to examine the proteins ARHGAP21, ARHGAP31, ARHGAP17, CDH2, IQGAP1, PACSIN2, PECAM1, TJP1, TJP2, TRIO, and TRIOBP for their potential roles related to their physical associations with N-cadherin. Affinity propagation clustering (Frey and Dueck, 2007) was used to autonomously group pro-

teins into clusters ( $n > 3$ ) based on the protein interaction matrix. Inter-cluster linkages were trimmed to include only those with strong support ( $>0.7$  confidence score). GO terms were obtained from BioMart, and associations were computed using the hypergeometric test ( $n > 5$ ) for each of the nine clusters containing the proteins of interest. Generic cellular structure GO terms such as “cytoplasm,” “membrane,” “nucleus,” etc. were excluded.

**R packages used.** The packages used were biomaRt, igraph, apcluster, parallel, RColorBrewer, RedeR, and ggplot2.

### Colocalization analysis of Trio and N-cadherin

Cells expressing GFP-Trio or GFP-Trio deletion mutants were immunoassayed for N-cadherin and imaged using a Zeiss LSM 880 microscope equipped with 63 $\times$  1.4 NA objective. The colocalization coefficient for GFP and N-cadherin was determined using z-stack images and Zen software according to the manufacturer’s instructions. Thresholded images were used to set the vertical and horizontal crosshairs to separate clusters into four quadrants (1: Trio<sup>+</sup>/N-cadherin<sup>-</sup>; 2: Trio<sup>-</sup>/N-cadherin<sup>+</sup>; 3: Trio<sup>+</sup>/N-cadherin<sup>+</sup>; and 4: Trio<sup>-</sup>/N-cadherin<sup>-</sup>). Cross-hair threshold values were set using cells expressing only GFP-Trio and not stained for N-cadherin or cells not expressing GFP-Trio and stained for N-cadherin. Colocalization analysis was done on a pixel-by-pixel basis. The Manders colocalization coefficient (Manders et al., 1992) was calculated as the sum of GFP-colocalized pixels (with N-cadherin-stained pixels) divided by the total number of GFP-Trio pixels.

### Quantification of pericyte coverage area in lung and brain

Fixed mouse lung or brain sections were costained for pericyte markers (PDGFR $\beta$  or desmin) and vessel markers (PECAM1 or laminin) and imaged using a Zeiss LSM 880 confocal microscope. The resultant z-stack was projected onto a two-dimensional plane. A threshold was used to eliminate background signal for each channel. The percent coverage was defined as the pixel area positive for both the pericyte and the vessel markers divided by the total vessel area in pixels (Armulik et al., 2010).

### Quantification of FRET/CFP ratio

For FRET analysis, a single confocal slice of the YFP image (at the junction or the abluminal surface) was used to create a binary mask with a value of 0 outside the cell and a value of 1 inside the cell. To generate a ratio image, the single-slice confocal FRET image was first multiplied by a binary mask image and then divided by the CFP image. The ratio images were rescaled to the lower value, and a linear pseudocolor table was applied to generate the color-coded image map. The integrated intensities for FRET and CFP within the region of interest were measured, and the relative activity of Rac1 and RhoA were expressed as mean pixel intensity of FRET/CFP ratio (Pertz et al., 2006).

### Statistics

Statistical significance calculations were performed using GraphPad Prism. A two-tailed, unpaired  $t$  test was used for experiments with two experimental groups and ANOVA for more than two experimental groups. Data distribution was assumed to be normal, but this was not formally tested. The following

notations are used throughout the text: ns,  $P > 0.05$ ; \*,  $P < 0.05$ ; \*\*,  $P < 0.01$ ; \*\*\*,  $P < 0.001$ ; and \*\*\*\*,  $P < 0.0001$ .

### Online supplemental material

Fig. S1 shows that genetic deletion of N-cadherin in ECs or pericytes induces vascular leakage. Fig. S2 shows that genetic deletion of N-cadherin in ECs or pericytes induces vascular leakage. Fig. S3 shows that genetic deletion of N-cadherin disassembles VE-cadherin adhesion. Fig. S4 shows that N-cadherin complexed with Trio signals assembly of VE-cadherin adhesion. Fig. S5 shows that N-cadherin complexed with Trio signals assembly of VE-cadherin adhesion. Fig. S6 shows that Trio GEF1 activity is required for assembly of VE-cadherin junctions downstream of N-cadherin signaling. Fig. S7 shows that activation of RhoA and increased intracellular tension are not sufficient to induce assembly of VE-cadherin junctions. Table S1 shows peptides identified in the N-cadherin mass spectrometry (MS) experiment. Table S2 shows GO terms from the N-cadherin MS experiment. Table S3 shows protein interaction scores from the N-cadherin MS experiment. Table S4 provides information regarding reagents and tools used in the paper.

### Acknowledgments

We thank Jaap van Buul (University of Amsterdam, Amsterdam, Netherlands) for GFP-Trio-FL, Trio-N, and Trio-C constructs; Klaus Hahn (University of North Carolina, Chapel Hill, NC) for RhoA and Rac1 biosensors; Martin A. Schwartz (Yale University, New Haven, CT) for overall discussion of the project; Joachim R. Gothert (West German Cancer Center, Essen, Germany) for end-SCL-Cre-ER<sup>T</sup>; Anne Debant (University of Montpellier, Montpellier, France) for Trio D1d and D2d mutants; Dr. Henar Cuervo (University of Illinois at Chicago [UIC], Chicago, IL) for PDGFR $\beta$ -P2A-CreER<sup>T2</sup> transgenic mice; Mr. Rohan Pisharody (UIC) for assistance with pericyte isolation and Western blotting; and the Taplin Mass Spectrometry Facility (Harvard University, Boston, MA) and the UIC Research Resource Center (Core Imaging Facility).

This work is supported by grants from the American Heart Association to K. Kruse (16PRE27260230) and X. Yang (17SDG33410608), and the National Institutes of Health to K. Kruse (T32HL007829-18), J. Klomp (T32HL007829-23), X. Yang (T32HL007829-23), Y.A. Komarova (R01HL103922 and P01 HL 060678, Core-5013), and L.M. Tai (R21AG053876).

The authors declare no competing financial interests.

Author contributions: Y.A. Komarova and K. Kruse conceived the project, interpreted data, and wrote the manuscript. K. Kruse performed all of the experiments, except those specifically attributed to other authors. Q.S. Lee and L.M. Tai performed immunofluorescence staining of lung and brain and calculated pericyte coverage; M.Y. Sun performed experiments with Rho activators; F. Huang isolated N-cadherin complexes; J. Klomp analyzed proteomics data; Y. Sun established the *Cdh2* iEC-KO model; S. Zhao established the *Cdh2* iPC-KO model and assisted with animal experiments; Z. Hong assisted with animal experiments; S.M. Vogel analyzed permeability times surface area product; X. Yang performed pulldown experiments; J.-W. Shin,

A.B. Malik, and D.E. Leckband provided critical discussion of the project; and A.B. Malik helped edit the manuscript.

Submitted: 14 February 2018

Revised: 10 June 2018

Accepted: 25 October 2018

### References

- Acharya, B.R., S.K. Wu, Z.Z. Lieu, R.G. Parton, S.W. Grill, A.D. Bershadsky, G.A. Gomez, and A.S. Yap. 2017. Mammalian Diaphanous 1 Mediates a Pathway for E-cadherin to Stabilize Epithelial Barriers through Junctional Contractility. *Cell Rep.* 18:2854–2867. <https://doi.org/10.1016/j.celrep.2017.02.078>
- Alanis-Lobato, G., M.A. Andrade-Navarro, and M.H. Schaefer. 2017. HIPPIE v2.0: enhancing meaningfulness and reliability of protein-protein interaction networks. *Nucleic Acids Res.* 45(D1):D408–D414. <https://doi.org/10.1093/nar/gkw985>
- Alimperti, S., T. Mirabella, V. Bajaj, W. Polacheck, D.M. Pirone, J. Duffield, J. Eyckmans, R.K. Assoian, and C.S. Chen. 2017. Three-dimensional biomimetic vascular model reveals a RhoA, Rac1, and N-cadherin balance in mural cell-endothelial cell-regulated barrier function. *Proc. Natl. Acad. Sci. USA.* 114:8758–8763. <https://doi.org/10.1073/pnas.1618333114>
- Armulik, A., A. Abramsson, and C. Betsholtz. 2005. Endothelial/pericyte interactions. *Circ. Res.* 97:512–523. <https://doi.org/10.1161/01.RES.0000182903.16652.d7>
- Armulik, A., G. Genové, M. Mäe, M.H. Nisancioglu, E. Wallgard, C. Niaudet, L. He, J. Norlin, P. Lindblom, K. Strittmatter, et al. 2010. Pericytes regulate the blood-brain barrier. *Nature.* 468:557–561. <https://doi.org/10.1038/nature09522>
- Armulik, A., G. Genové, and C. Betsholtz. 2011. Pericytes: developmental, physiological, and pathological perspectives, problems, and promises. *Dev. Cell.* 21:193–215. <https://doi.org/10.1016/j.devcel.2011.07.001>
- Baeyens, N., C. Bandyopadhyay, B.G. Coon, S. Yun, and M.A. Schwartz. 2016. Endothelial fluid shear stress sensing in vascular health and disease. *J. Clin. Invest.* 126:821–828. <https://doi.org/10.1172/JCI83083>
- Boroujerdi, A., U. Tigges, J.V. Welser-Alves, and R. Milner. 2014. Isolation and culture of primary pericytes from mouse brain. *Methods Mol. Biol.* 1135:383–392. [https://doi.org/10.1007/978-1-4939-0320-7\\_31](https://doi.org/10.1007/978-1-4939-0320-7_31)
- Bouquier, N., E. Vignal, S. Charrasse, M. Weill, S. Schmidt, J.P. Léonetti, A. Blangy, and P. Fort. 2009. A cell active chemical GEF inhibitor selectively targets the Trio/RhoG/Rac1 signaling pathway. *Chem. Biol.* 16:657–666. <https://doi.org/10.1016/j.chembiol.2009.04.012>
- Carmeliet, P., M.G. Lampugnani, L. Moons, F. Breviario, V. Compernelle, F. Bono, G. Balconi, R. Spagnuolo, B. Oosthuysen, M. Dewerchin, et al. 1999. Targeted deficiency or cytosolic truncation of the VE-cadherin gene in mice impairs VEGF-mediated endothelial survival and angiogenesis. *Cell.* 98:147–157. [https://doi.org/10.1016/S0092-8674\(00\)81010-7](https://doi.org/10.1016/S0092-8674(00)81010-7)
- Chang, J., M.R. Mancuso, C. Maier, X. Liang, K. Yuki, L. Yang, J.W. Kwong, J. Wang, V. Rao, M. Vallon, et al. 2017. Gpr124 is essential for blood-brain barrier integrity in central nervous system disease. *Nat. Med.* 23:450–460. <https://doi.org/10.1038/nm.4309>
- Charrasse, S., M. Meriane, F. Comunale, A. Blangy, and C. Gauthier-Rouvière. 2002. N-cadherin-dependent cell-cell contact regulates Rho GTPases and beta-catenin localization in mouse C2C12 myoblasts. *J. Cell Biol.* 158:953–965. <https://doi.org/10.1083/jcb.200202034>
- Charrasse, S., F. Comunale, M. Fortier, E. Portales-Casamar, A. Debant, and C. Gauthier-Rouvière. 2007. M-cadherin activates Rac1 GTPase through the Rho-GEF trio during myoblast fusion. *Mol. Biol. Cell.* 18:1734–1743. <https://doi.org/10.1091/mbc.e06-08-0766>
- Chevalier, S., C. Cuestas-Ayllon, V. Grazu, M. Luna, H. Feracci, and J.M. de la Fuente. 2010. Creating biomimetic surfaces through covalent and oriented binding of proteins. *Langmuir.* 26:14707–14715. <https://doi.org/10.1021/la103086b>
- Comunale, F., M. Causeret, C. Favard, J. Cau, N. Taulet, S. Charrasse, and C. Gauthier-Rouvière. 2007. Rac1 and RhoA GTPases have antagonistic functions during N-cadherin-dependent cell-cell contact formation in C2C12 myoblasts. *Biol. Cell.* 99:503–517. <https://doi.org/10.1042/BC20070011>
- Cosgrove, B.D., K.L. Mui, T.P. Driscoll, S.R. Caliari, K.D. Mehta, R.K. Assoian, J.A. Burdick, and R.L. Mauck. 2016. N-cadherin adhesive interactions modulate matrix mechanosensing and fate commitment of mesen-



- chymal stem cells. *Nat. Mater.* 15:1297–1306. <https://doi.org/10.1038/nmat4725>
- Courtroy, P.J., and J. Boyles. 1983. Fibronectin in the microvasculature: localization in the pericyte-endothelial interstitium. *J. Ultrastruct. Res.* 83:258–273. [https://doi.org/10.1016/S0022-5320\(83\)90133-8](https://doi.org/10.1016/S0022-5320(83)90133-8)
- Cuervo, H., B. Pereira, T. Nadeem, M. Lin, F. Lee, J. Kitajewski, and C.S. Lin. 2017. PDGFR $\beta$ -P2A-CreER<sup>T2</sup> mice: a genetic tool to target pericytes in angiogenesis. *Angiogenesis*. 20:655–662. <https://doi.org/10.1007/s10456-017-9570-9>
- Daneman, R., L. Zhou, A.A. Kebede, and B.A. Barres. 2010. Pericytes are required for blood-brain barrier integrity during embryogenesis. *Nature*. 468:562–566. <https://doi.org/10.1038/nature09513>
- Daneshjoui, N., N. Sieracki, G.P. van Nieuw Amerongen, D.E. Conway, M.A. Schwartz, Y.A. Komarova, and A.B. Malik. 2015. Rac1 functions as a reversible tension modulator to stabilize VE-cadherin trans-interaction. *J. Cell Biol.* 208:23–32. <https://doi.org/10.1083/jcb.201409108>
- Debant, A., C. Serra-Pagès, K. Seipel, S. O'Brien, M. Tang, S.H. Park, and M. Streuli. 1996. The multidomain protein Trio binds the LAR transmembrane tyrosine phosphatase, contains a protein kinase domain, and has separate rac-specific and rho-specific guanine nucleotide exchange factor domains. *Proc. Natl. Acad. Sci. USA.* 93:5466–5471. <https://doi.org/10.1073/pnas.93.11.5466>
- Del Vecchio, P.J., A. Siflinger-Birnboim, J.M. Shepard, R. Bizios, J.A. Cooper, and A.B. Malik. 1987. Endothelial monolayer permeability to macromolecules. *Fed. Proc.* 46:2511–2515.
- Frey, B.J., and D. Dueck. 2007. Clustering by passing messages between data points. *Science*. 315:972–976. <https://doi.org/10.1126/science.1136800>
- Frye, M., M. Dierkes, V. Küppers, M. Vockel, J. Tomm, D. Zeuschner, J. Rossaint, A. Zarbock, G.Y. Koh, K. Peters, et al. 2015. Interfering with VE-PTP stabilizes endothelial junctions in vivo via Tie-2 in the absence of VE-cadherin. *J. Exp. Med.* 212:2267–2287. <https://doi.org/10.1084/jem.20150718>
- García-Mata, R., K. Wennerberg, W.T. Arthur, N.K. Noren, S.M. Ellerbroek, and K. Burridge. 2006. Analysis of activated GAPs and GEFs in cell lysates. *Methods Enzymol.* 406:425–437. [https://doi.org/10.1016/S0076-6879\(06\)06031-9](https://doi.org/10.1016/S0076-6879(06)06031-9)
- Gerhardt, H., H. Wolburg, and C. Redies. 2000. N-cadherin mediates pericyte-endothelial interaction during brain angiogenesis in the chicken. *Dev. Dyn.* 218:472–479. [https://doi.org/10.1002/1097-0177\(200007\)218:3%3C472::AID-DVDY1008%3E3.0.CO;2-#](https://doi.org/10.1002/1097-0177(200007)218:3%3C472::AID-DVDY1008%3E3.0.CO;2-#)
- Göthert, J.R., S.E. Gustin, J.A. van Eekelen, U. Schmidt, M.A. Hall, S.M. Jane, A.R. Green, B. Göttgens, D.J. Izon, and C.G. Begley. 2004. Genetically tagging endothelial cells in vivo: bone marrow-derived cells do not contribute to tumor endothelium. *Blood*. 104:1769–1777. <https://doi.org/10.1182/blood-2003-11-3952>
- Gu, H., J.D. Marth, P.C. Orban, H. Mossmann, and K. Rajewsky. 1994. Deletion of a DNA polymerase beta gene segment in T cells using cell type-specific gene targeting. *Science*. 265:103–106. <https://doi.org/10.1126/science.8016642>
- Hatta, K., A. Nose, A. Nagafuchi, and M. Takeichi. 1988. Cloning and expression of cDNA encoding a neural calcium-dependent cell adhesion molecule: its identity in the cadherin gene family. *J. Cell Biol.* 106:873–881. <https://doi.org/10.1083/jcb.106.3.873>
- Itoh, F., S. Itoh, T. Adachi, K. Ichikawa, Y. Matsumura, T. Takagi, M. Festing, T. Watanabe, M. Weinstein, S. Karlsson, and M. Kato. 2012. Smad2/Smad3 in endothelium is indispensable for vascular stability via S1PR1 and N-cadherin expressions. *Blood*. 119:5320–5328. <https://doi.org/10.1182/blood-2011-12-395772>
- Kashef, J., A. Köhler, S. Kuriyama, D. Alfandari, R. Mayor, and D. Wedlich. 2009. Cadherin-11 regulates protrusive activity in Xenopus cranial neural crest cells upstream of Trio and the small GTPases. *Genes Dev.* 23:1393–1398. <https://doi.org/10.1101/gad.519409>
- Kawedia, J.D., M.L. Nieman, G.P. Boivin, J.E. Melvin, K. Kikuchi, A.R. Hand, J.N. Lorenz, and A.G. Menon. 2007. Interaction between transcellular and paracellular water transport pathways through Aquaporin 5 and the tight junction complex. *Proc. Natl. Acad. Sci. USA.* 104:3621–3626. <https://doi.org/10.1073/pnas.0608384104>
- Komarova, Y.A., F. Huang, M. Geyer, N. Daneshjoui, A. Garcia, L. Idalino, B. Kreutz, D. Mehta, and A.B. Malik. 2012. VE-cadherin signaling induces EB3 phosphorylation to suppress microtubule growth and assemble adherens junctions. *Mol. Cell.* 48:914–925. <https://doi.org/10.1016/j.molcel.2012.10.011>
- Komarova, Y.A., K. Kruse, D. Mehta, and A.B. Malik. 2017. Protein Interactions at Endothelial Junctions and Signaling Mechanisms Regulating Endothelial Permeability. *Circ. Res.* 120:179–206. <https://doi.org/10.1161/CIRCRESAHA.116.306534>
- Lampugnani, M.G., M. Resnati, M. Raiteri, R. Pigott, A. Pisacane, G. Houen, L.P. Ruco, and E. Dejana. 1992. A novel endothelial-specific membrane protein is a marker of cell-cell contacts. *J. Cell Biol.* 118:1511–1522. <https://doi.org/10.1083/jcb.118.6.1511>
- Leonard, M., L. Zhang, N. Zhai, A. Cader, Y. Chan, R.B. Nowak, V.M. Fowler, and A.S. Menko. 2011. Modulation of N-cadherin junctions and their role as epicenters of differentiation-specific actin regulation in the developing lens. *Dev. Biol.* 349:363–377. <https://doi.org/10.1016/j.ydbio.2010.10.009>
- Li, F., Y. Lan, Y. Wang, J. Wang, G. Yang, F. Meng, H. Han, A. Meng, Y. Wang, and X. Yang. 2011. Endothelial Smad4 maintains cerebrovascular integrity by activating N-cadherin through cooperation with Notch. *Dev. Cell.* 20:291–302. <https://doi.org/10.1016/j.devcel.2011.01.011>
- Luo, Y., and G.L. Radice. 2005. N-cadherin acts upstream of VE-cadherin in controlling vascular morphogenesis. *J. Cell Biol.* 169:29–34. <https://doi.org/10.1083/jcb.200411127>
- MacNevin, C.J., A. Touchkine, D.J. Marston, C.W. Hsu, D. Tsygankov, L. Li, B. Liu, T. Qi, D.V. Nguyen, and K.M. Hahn. 2016. Ratiometric Imaging Using a Single Dye Enables Simultaneous Visualization of Rac1 and Cdc42 Activation. *J. Am. Chem. Soc.* 138:2571–2575. <https://doi.org/10.1021/jacs.5b09764>
- Manders, E.M., J. Stap, G.J. Brakenhoff, R. van Driel, and J.A. Aten. 1992. Dynamics of three-dimensional replication patterns during the S-phase, analysed by double labelling of DNA and confocal microscopy. *J. Cell Sci.* 103:857–862.
- Mary, S., S. Charrasse, M. Meriane, F. Comunale, P. Travo, A. Blangy, and C. Gauthier-Rouvière. 2002. Biogenesis of N-cadherin-dependent cell-cell contacts in living fibroblasts is a microtubule-dependent kinesin-driven mechanism. *Mol. Biol. Cell.* 13:285–301. <https://doi.org/10.1091/mbc.01-07-0337>
- Medley, Q.G., E.G. Buchbinder, K. Tachibana, H. Ngo, C. Serra-Pagès, and M. Streuli. 2003. Signaling between focal adhesion kinase and trio. *J. Biol. Chem.* 278:13265–13270. <https://doi.org/10.1074/jbc.M300277200>
- Mehta, D., and A.B. Malik. 2006. Signaling mechanisms regulating endothelial permeability. *Physiol. Rev.* 86:279–367. <https://doi.org/10.1152/physrev.00012.2005>
- Navarro, P., L. Ruco, and E. Dejana. 1998. Differential localization of VE- and N-cadherins in human endothelial cells: VE-cadherin competes with N-cadherin for junctional localization. *J. Cell Biol.* 140:1475–1484. <https://doi.org/10.1083/jcb.140.6.1475>
- Paik, J.H., A. Skoura, S.S. Chae, A.E. Cowan, D.K. Han, R.L. Proia, and T. Hla. 2004. Sphingosine 1-phosphate receptor regulation of N-cadherin mediates vascular stabilization. *Genes Dev.* 18:2392–2403. <https://doi.org/10.1101/gad.1227804>
- Pertz, O., L. Hodgson, R.L. Klemke, and K.M. Hahn. 2006. Spatiotemporal dynamics of RhoA activity in migrating cells. *Nature*. 440:1069–1072. <https://doi.org/10.1038/nature04665>
- Pinter, G.G., J.L. Atkins, and D.R. Bell. 1974. Albumin permeability times surface area (PS) product of peritubular capillaries in kidney. *Experientia*. 30:1045. <https://doi.org/10.1007/BF01939000>
- Quadri, S.K., L. Sun, M.N. Islam, L. Shapiro, and J. Bhattacharya. 2012. Cadherin selectivity filter regulates endothelial sieving properties. *Nat. Commun.* 3:1099. <https://doi.org/10.1038/ncomms2107>
- Salomon, D., O. Ayalon, R. Patel-King, R.O. Hynes, and B. Geiger. 1992. Extrajunctional distribution of N-cadherin in cultured human endothelial cells. *J. Cell Sci.* 102:7–17.
- Scott, D.W., C.E. Tolbert, and K. Burridge. 2016. Tension on JAM-A activates RhoA via GEF-H1 and p115 RhoGEF. *Mol. Biol. Cell.* 27:1420–1430. <https://doi.org/10.1091/mbc.e15-12-0833>
- Seipel, K., Q.G. Medley, N.L. Kedersha, X.A. Zhang, S.P. O'Brien, C. Serra-Pages, M.E. Hemler, and M. Streuli. 1999. Trio amino-terminal guanine nucleotide exchange factor domain expression promotes actin cytoskeleton reorganization, cell migration and anchorage-independent cell growth. *J. Cell Sci.* 112:1825–1834.
- Seipel, K., S.P. O'Brien, E. Iannotti, Q.G. Medley, and M. Streuli. 2001. Tara, a novel F-actin binding protein, associates with the Trio guanine nucleotide exchange factor and regulates actin cytoskeletal organization. *J. Cell Sci.* 114:389–399.
- Siddiqui, M.R., Y.A. Komarova, S.M. Vogel, X. Gao, M.G. Bonini, J. Rajasingh, Y.Y. Zhao, V. Brovkovich, and A.B. Malik. 2011. Caveolin-1-eNOS signaling promotes p190RhoGAP-A nitration and endothelial permeability. *J. Cell Biol.* 193:841–850. <https://doi.org/10.1083/jcb.201012129>
- Simionescu, M., N. Simionescu, and G.E. Palade. 1975. Segmental differentiations of cell junctions in the vascular endothelium. The microvasculature. *J. Cell Biol.* 67:863–885. <https://doi.org/10.1083/jcb.67.3.863>

- Straight, A.F., A. Cheung, J. Limouze, I. Chen, N.J. Westwood, J.R. Sellers, and T.J. Mitchison. 2003. Dissecting temporal and spatial control of cytokinesis with a myosin II Inhibitor. *Science*. 299:1743–1747. <https://doi.org/10.1126/science.1081412>
- Tillet, E., D. Vittet, O. Féraud, R. Moore, R. Kemler, and P. Huber. 2005. N-cadherin deficiency impairs pericyte recruitment, and not endothelial differentiation or sprouting, in embryonic stem cell-derived angiogenesis. *Exp. Cell Res.* 310:392–400. <https://doi.org/10.1016/j.yexcr.2005.08.021>
- Timmerman, I., N. Heemskerk, J. Kroon, A. Schaefer, J. van Rijssel, M. Hoogenboezem, J. van Unen, J. Goedhart, T.W. Gadella Jr., T. Yin, et al. 2015. A local VE-cadherin and Trio-based signaling complex stabilizes endothelial junctions through Rac1. *J. Cell Sci.* 128:3041–3054. <https://doi.org/10.1242/jcs.168674>
- van Rijssel, J., J. Kroon, M. Hoogenboezem, F.P. van Alphen, R.J. de Jong, E. Kostadinova, D. Geerts, P.L. Hordijk, and J.D. van Buul. 2012. The Rho-guanine nucleotide exchange factor Trio controls leukocyte transendothelial migration by promoting docking structure formation. *Mol. Biol. Cell.* 23:2831–2844. <https://doi.org/10.1091/mbc.e11-11-0907>
- Weisberg, H.F. 1978. Osmotic pressure of the serum proteins. *Ann. Clin. Lab. Sci.* 8:155–164.
- Wu, Y.I., D. Frey, O.I. Lungu, A. Jaehrig, I. Schlichting, B. Kuhlman, and K.M. Hahn. 2009. A genetically encoded photoactivatable Rac controls the motility of living cells. *Nature*. 461:104–108. <https://doi.org/10.1038/nature08241>
- Yano, H., Y. Mazaki, K. Kurokawa, S.K. Hanks, M. Matsuda, and H. Sabe. 2004. Roles played by a subset of integrin signaling molecules in cadherin-based cell-cell adhesion. *J. Cell Biol.* 166:283–295. <https://doi.org/10.1083/jcb.200312013>
- Yano, T., Y. Yamazaki, M. Adachi, K. Okawa, P. Fort, M. Uji, S. Tsukita, and S. Tsukita. 2011. Tara up-regulates E-cadherin transcription by binding to the Trio RhoGEF and inhibiting Rac signaling. *J. Cell Biol.* 193:319–332. <https://doi.org/10.1083/jcb.201009100>
- Yarrow, J.C., G. Totsukawa, G.T. Charras, and T.J. Mitchison. 2005. Screening for cell migration inhibitors via automated microscopy reveals a Rho-kinase inhibitor. *Chem. Biol.* 12:385–395. <https://doi.org/10.1016/j.chembiol.2005.01.015>
- Zeng, H., X. He, Q.H. Tuo, D.F. Liao, G.Q. Zhang, and J.X. Chen. 2016. LPS causes pericyte loss and microvascular dysfunction via disruption of Sirt3/angiopoietins/Tie-2 and HIF-2 $\alpha$ /Notch3 pathways. *Sci. Rep.* 6:20931;1–13. <https://doi.org/10.1038/srep20931>